Available online at www.sciencedirect.com
ScienceDirect
Geochimica et Cosmochimica Acta 70 (2006) 4617–4634
Geochimica
www.elsevier.com/locate/gca

Element partitioning during precipitation of aragonite from seawater: A framework for understanding paleoproxies

Glenn A. Gaetani *, Anne L. Cohen

Department of Geology and Geophysics, Woods Hole Oceanographic Institution, Woods Hole, MA 02543, USA

Received 17 January 2006; accepted in revised form 10 July 2006

Abstract

This study presents the results from precipitation experiments carried out to investigate the partitioning of the alkaline earth cations Mg^{2+}, Ca^{2+}, Sr^{2+}, and Ba^{2+} between abiogenic aragonite and seawater as a function of temperature. Experiments were carried out at 5 to 75 °C, using the protocol of Kinsman and Holland [Kinsman, D.J.J., Holland, H.D., 1969. The coprecipitation of cations with $CaCO_3$: IV. The coprecipitation of Sr^{2+} with aragonite between 16 and 96 °C. *Geochim. Cosmochim. Acta* **33**, 1–17.] The concentrations of Mg, Sr, and Ba were determined in the fluid from each experiment by inductively coupled plasma-mass spectrometry, and in individual aragonite grains by secondary ion mass spectrometry. The experimentally produced aragonite grains are enriched in trace components (''impurities'') relative to the concentrations expected from crystal-fluid equilibrium, indicating that kinetic processes are controlling element distribution. Our data are not consistent with fractionations produced kinetically in a boundary layer adjacent to the growing crystal because Sr^{2+}, a compatible element, is enriched rather than depleted in the aragonite. Element compatibilities, and the systematic change in partitioning with temperature, can be explained by the process of surface entrapment proposed by Watson and Liang [Watson, E.B., Liang, Y., 1995. A simple model for sector zoning in slowly grown crystals: implications for growth rate and lattice diffusion, with emphasis on accessory minerals in crustal rocks. *Am. Mineral.* **80**, 1179–1187] and Watson [Watson, E.B., 1996. Surface enrichment and trace-element uptake during crystal growth. *Geochim. Cosmochim. Acta* **60**, 5013–5020; Watson, E.B., 2004. A conceptual model for near-surface kinetic controls on the trace-element and stable isotope composition of abiogenic calcite crystals. *Geochim. Cosmochim. Acta* **68**, 1473–1488]. This process is thought to operate in regimes where the competition between crystal growth rate and diffusivity in the near-surface region limits the extent to which the solid can achieve partitioning equilibrium with the fluid. A comparison of the skeletal composition of *Diploria labyrinthiformis* (brain coral) collected on Bermuda with results from precipitation calculations carried out using our experimentally determined partition coefficients indicate that the fluid from which coral skeleton precipitates has a Sr/Ca ratio comparable to that of seawater, but is depleted in Mg and Ba, and that there are seasonal fluctuations in the mass fraction of aragonite precipitated from the calcifying fluid (''precipitation efficiency''). The combined effects of surface entrapment during aragonite growth and seasonal fluctuations in ''precipitation efficiency'' likely forms the basis for the temperature information recorded in the aragonite skeletons of Scleractinian corals.

1. Introduction

The elemental composition of biogenic (or biologically precipitated) aragonite is an important tool for paleoclimate studies. The relationship between the Sr/Ca ratio of coral skeleton and sea surface temperature (SST) is a widely used means for deriving high-resolution proxy records (Smith et al., 1979), and has been employed to study many important periods in Earth's climate history, including the Last Interglacial, Last Glacial Maximum, the Younger Dryas, and the Little Ice Age (e.g., Guilderson et al., 1994; Beck et al., 1997; Winter et al., 2000; Tudhope et al., 2001; Watanabe et al., 2001; Correge et al., 2004; Felis et al., 2004). Since the development of Sr/Ca paleothermometry, the exploitation of elemental proxies has broadened considerably to include such elements as Mg,

* Corresponding author. Fax: +1 508 457 2183.
E-mail address: ggaetani@whoi.edu (G.A. Gaetani).

0016-7037/$ - see front matter © 2006 Elsevier Inc. All rights reserved.
doi:10.1016/j.gca.2006.07.008

Ba, U, and Cd (Min et al., 1995; Shen and Dunbar, 1995; Mitsuguchi et al., 1996; Watanabe et al., 2001; Alibert et al., 2003; McCulloch et al., 2003; Reuer et al., 2003). This growth has occurred for three reasons: (1) elemental thermometers are considered particularly useful because, unlike oxygen isotope ratios ($\delta^{18}O$), the trace element composition of the ocean is thought to remain relatively constant on decadal through millennial timescales (e.g., Beck et al., 1992); (2) the diversity of elemental tracers has the potential to encompass a broad array of environmental variables (e.g., Lea, 2003); and (3) technological advances in analytical techniques enable large amounts of data to be efficiently collected from a single sample with high precision and spatial resolution (e.g., Schrag, 1999). Paleoceanographic reconstructions are typically derived from biogenic carbonates using empirical relationships between elemental ratios and environmental variables calibrated using the skeletons of organisms grown under known conditions (e.g., Swart et al., 2002; Cohen et al., 2004; Rosenheim et al., 2004). These relationships are applied to modern specimens or samples from the fossil record to reconstruct temperature, salinity, and circulation patterns of the environments in which they grew.

While this approach has produced significant advances in paleoclimatology, its accuracy is limited by the ambiguity inherent in relationships derived empirically from living organisms. Our understanding of the factors that control how specific elements are distributed, or partitioned, between seawater and a growing carbonate skeleton is extremely limited or, in some cases, entirely lacking. The need for new experimental data relating to element partitioning between abiogenic aragonite and seawater is exemplified by the unexplained range of elemental ratio-temperature relationships derived for different aragonite-secreting organisms, from mollusks to fish to corals to sclerosponges, and the existence of high amplitude, high frequency variations in element ratios in skeletal aragonite that cannot be explained by temperature (e.g., Cohen et al., 2001; Meibom et al., 2004; Sinclair, 2005).

Here, we present the results from precipitation experiments carried out to investigate the partitioning of the alkaline earth cations Mg^{2+}, Ca^{2+}, Sr^{2+}, and Ba^{2+} between abiogenic aragonite and seawater as a function of temperature. Results from these experiments show that the Mg/Ca, Sr/Ca, and Ba/Ca ratios of abiogenic aragonite are inversely correlated with temperature, and that Ba/Ca has the strongest temperature sensitivity. The experimentally determined partitioning of Mg^{2+}, Ca^{2+}, Sr^{2+}, and Ba^{2+} between aragonite and seawater are not consistent with either equilibrium thermodynamics or kinetic fractionations produced in a fluid boundary layer adjacent to the growing crystal. Rather, the compatibilities of these elements, and the systematic change in partitioning with temperature, can be explained by the process of surface entrapment proposed by Watson and Liang (1995) and Watson (1996, 2004). A comparison of the skeletal composition of *Diploria labyrinthiformis* (brain coral) collected on Bermuda with results from calculations carried out using our experimentally determined partition coefficients indicate that the fluid from which coral skeleton precipitates has a Sr/Ca ratio close to that of seawater, but that the Mg/Ca and Ba/Ca ratios are significantly depleted relative to seawater and that there are seasonal fluctuations in the mass fraction of aragonite precipitated from the calcifying fluid (“precipitation efficiency”). The combined effects of surface entrapment during aragonite growth and seasonal fluctuations in “precipitation efficiency” likely forms the basis for the temperature information recorded in the aragonite skeletons of Scleractinian corals.

2. Experimental and analytical methods

The seawater used in the experiments was collected from Vineyard Sound, Massachusetts, passed through a 0.45 μm filter and stored in the dark. Experiments were performed by first placing 600 ml of seawater into a covered beaker made from Teflon fluorocarbon resin (PTFE). The seawater was equilibrated at the desired temperature by placing the beaker into a Lauda RE-106 isothermal bath for ~1–2 h, while continuously stirring at 120 rpm. Once the seawater reached the desired temperature, 125 ml of 0.01 m aqueous Na_2CO_3 solution was added, drop-wise, at a rate of ~1 ml/min using a low-flow peristaltic pump. This solution was prepared by dissolving 300 mg of high purity Na_2CO_3 powder in 250 ml of distilled water. A second 125 ml aliquot of the solution was added to the experiment ~19–24 h after the first, by the same method. Total experimental durations ranged between 91 and 168 h from the addition of the first aliquot of Na_2CO_3 solution.

Following each experiment, the fluid was filtered (particle retention size >3 μm) to remove any precipitate that remained in suspension, and analyzed for ^{25}Mg, ^{48}Ca, ^{86}Sr, and ^{138}Ba using the Thermo-Finnigan Element2 inductively coupled plasma-mass spectrometer (ICP-MS) at Woods Hole Oceanographic Institution. All measurements were made at medium resolution. Indium was used as an internal standard at a concentration of 2.17 ppb; count rates for ^{115}In over the course of this study were 34000 ± 3000 cps/ppb. Blank values, in percent relative, were 0.0006 for ^{25}Mg, 0.09 for ^{48}Ca, 0.06 for ^{86}Sr, and 3.2 for ^{138}Ba.

Total alkalinity (TA) was analyzed by automated Gran titration of 1.5 ml samples (Gieskes and Rogers, 1973). The analyses were calibrated using certified reference seawater samples supplied by A.G. Dickson (SIO). Precision was ±10 μmol/kg.

Total CO_2 (TCO_2) was analyzed by an automated system in which 0.3 ml samples are acidified with 2 ml of 1% H_3PO_4 and the CO_2 evolved is stripped with N_2 gas and analyzed by infrared absorption using a LICOR-6252 infrared analyzer. The procedure is based on O’Sullivan and Millero (1998). The instrument was calibrated using certified reference seawater samples supplied by A.G. Dickson (SIO). Precision was ±5 μmol/kg.

Salinity (S) measurements were performed using a Guildline autosal model 8400B salinometer. Samples are maintained at room temperature (22 °C) before measurement; the autosal's bath temperature is set at 24 °C. IAPSO standard seawater (current batch, P-143) is used to standardize the autosal before runs. The accuracy of a salinity measurement is estimated to be ±0.003 psu, with a resolution of 0.0002 at 35 psu.

Crystals that precipitated over the course of an experiment were removed from the filter paper, beaker, and stirring rod, mounted in epoxy, and polished for visual inspection. X-ray powder diffraction was used to identify an aliquot of the precipitate as aragonite. The Mg/Ca, Sr/Ca, and Ba/Ca ratios of individual crystals were determined by secondary ion mass spectrometry (SIMS) using the Cameca 3f ion microprobe at Woods Hole Oceanographic Institution. Individual spherulites were targeted with a 4 nA primary O^- beam, 10-μm in diameter, accelerated at 12.5 keV. Following a 3 min pre-burn to remove the Au coat, a single spot was occupied while measuring secondary ion intensities for ^{24}Mg, ^{42}Ca, ^{88}Sr, and ^{138}Ba within a 30 eV window centered on an 80 eV offset from the peak of the energy distribution. This energy filtering reduces molecular interferences to <0.1%. The mass spectra for Mg, Ca, Sr, and Ba were determined to be free from significant isobaric interferences through a comparison of measured isotope ratios with natural abundances (Hart and Cohen, 1996). Isotope ratios were converted to molar ratios using a carbonatite standard (OKA) with Mg/Ca, Sr/Ca, and Ba/Ca ratios determined by solution ICP-MS to be 4.47, 19.3, and 1.61 mmol/mol, respectively. Elemental ratios derived from the SIMS analyses were converted to concentration using analyses of Ca (1σ uncertainties <1% relative) carried out on the JEOL 733 electron microprobe at the Massachusetts Institute of Technology. These analyses were performed using a beam current of 10 nA and an accelerating potential of 15 keV.

Details of elemental analyses of *Diploria* skeleton are given in Cohen et al. (2004). Briefly, ratios of masses $^{24}Mg/^{42}Ca$, $^{88}Sr/^{42}Ca$, and $^{138}Ba/^{42}Ca$ were determined using a Cameca 3f ion microprobe employing SIMS techniques and converted to molar ratios using the OKA standard. The ion microprobe enables *in situ* elemental analyses of intact coral skeleton to be made at micron-scale resolution by targeting discrete crystal bundles within skeletal elements of the corallite. In this study we used a 5 nA O^- beam to sputter the surface of an epoxy-mounted polished section of skeleton that was removed from the maximum growth axis of the stained colony. Routine instrument precision for $^{24}Mg/^{42}Ca$, $^{88}Sr/^{42}Ca$, and $^{138}Ba/^{42}Ca$ are 1.2%, 0.3%, and 4% (2σ) respectively. Sample spots of 20 μm diameter were analyzed at 100 μm intervals. To avoid thickening deposits, a sample track was followed close to centers of calcification down the length of a septum within the ambulacrum. Data filtering was carried out as described in Cohen and Reves-Sohn (2004).

Details of the *Diploria* staining procedure are given in Cohen et al. (2004). Briefly, a small (~50 mm height) colony of *D. labyrinthiformis* growing at 50 ft depth on the south terrace of the Bermuda platform was stained with sodium alizarin sulphonate over a period of one year. The colony was collected live in June 2000 and placed in shaded, aerated flow-through seawater aquaria for two days. The stain (15 mg/L) was introduced to the aquaria for 24 h, flushed, and the coral allowed to recover for 2 days. It was then returned to the study site and re-attached to the substratum with an underwater cement (7:1 mixture of Portland Type II cement and Plaster of Paris). The colony was stained again on September 18th, 2000 and January 24th, 2001 and collected on June 1st, 2001.

3. Results

Experiments carried out at temperatures of 5–75 °C produced precipitates consisting of either calcite or aragonite (Table 1). The latter is metastable with respect to calcite at the conditions of our experiments, but is kinetically favored as a precipitate from seawater (e.g., Burton and Walter, 1987; Morse et al., 1997). Therefore, references throughout the text to an equilibrium state refer to metastable equilibrium involving aragonite and seawater. The seawater used in the experiments had S of 32.0 psu and

Table 1
Experimental conditions

Expt	Temperature (°C)	Duration (h)	Precipitate (wt%)	$pH_{Initial}$	$\Omega_{Initial}$ (calcite)	$\Omega_{Initial}$ (aragonite)
ASW-6	5	189	0.0315(4)	9.65	69.2	41.9
ASW-4	15	96	0.0215(4)	9.50	71.1	43.9
ASW-1	25	96.5	0.0271(3)	9.35	73.9	46.7
ASW-2	35	168	0.0288(4)	9.21	78.5	51.1
ASW-3	45	91	0.0290(4)	9.08	84.6	57.1
ASW-7	55	120	0.0318(6)	8.96	92.9	65.5
ASW-8	65	120	0.0336(5)	8.84	103.5	76.4
ASW-9	75	146	0.0334(10)	8.73	117.3	91.1

Notes: The amount of aragonite precipitated in each experiment was calculated using a weighted mass balance of the concentrations of Mg, Ca, Sr, and Ba in fluid and solid. Units in parentheses represent 1 standard error in terms of least units cited based on propogation of analytical uncertainties. Therefore, 0.0315(4) should be read as 0.0315 ± 0.0004. Estimates for the initial pH and Ω of each experiment were calculated based on TA and TCO2 using the algorithm written by D. Pierrot and F.J. Millero that uses the constants of Millero et al. (2006). In these calculations it was assumed that no aragonite precipitated prior to complete addition of the second aliquot of aqueous Na_2CO_3 solution.

Table 2
Element concentrations in starting materials and experimental fluids

Fluid	S	TA	TCO_2	Mg	Ca	Sr	Ba
Seawater	32.032	2144	2005	1249(9)	394(3)	7.28(6)	7.08(21)
ASW-6	22.952	3415	—	875(8)	202(2)	3.83(3)	3.11(6)
ASW-4	23.153	3538	—	883(4)	201(1)	3.36(1)	2.20(5)
ASW-1	23.080	2602	—	859(5)	171(1)	3.01(1)	2.87(8)
ASW-2	23.525	2152	—	894(8)	167(1)	3.00(2)	3.02(8)
ASW-3	23.544	1695	—	906(7)	166(2)	3.03(1)	3.66(5)
ASW-7	23.810	1465	—	916(9)	161(2)	3.09(3)	3.81(5)
ASW-8	24.336	1138	—	935(6)	154(1)	3.05(1)	4.30(8)
ASW-9	27.229	1006	—	994(8)	172(1)	3.54(1)	5.16(8)

Notes: Salinity is reported in practical salinity units (psu). Accuracy of the salinity measurements is estimated to be ±0.003 psu. Alkalinity (TA) and total CO_2 (TCO_2) are reported in units of μmol/kg. Precision of the alkalinity measurements is estimated to be ±5 μmol/kg based on replicate analyses. Precision of the total CO_2 measurements is estimated to be ±3 μmol/kg based on replicate analyses. Mg, Ca, and Sr concentrations are reported in ppm; Ba concentrations are reported in ppb. Each reported trace element concentration represents the mean of five individual ICP-MS analyses. Units in parentheses represent 1 standard deviation in terms of least units cited, on the basis of replicate analyses. Therefore, 1249(9) should be read as 1249 ± 9.

TA of 2144 μmol/kg (Table 2); its saturation state (Ω) with respect to calcite and aragonite at 25 °C were 3.1 and 2.0, respectively. The addition of 250 ml of 0.01 m aqueous Na_2CO_3 solution at the beginning of each experiment decreased S to ~23 psu and increased TA to ~7396 μmol/kg. The experiment carried out at 5 °C had an initial Ω with respect to calcite of 69.2 and precipitated 0.0315 ± 0.0004 wt% calcite. The concentration of Mg in this calcite is 1.90 ± 0.04 wt%. Experiments carried out at 15–75 °C had initial Ω with respect to aragonite that increased from 43.9 to 91.1 with increasing experimental temperature (Table 1). The mass of aragonite precipitated in these experiments varies systematically from 0.0215 ± 0.0004 wt% at 15 °C and $\Omega_{Initial} = 43.9$ to 0.0334 ± 0.0010 wt% at 75 °C and $\Omega_{Initial} = 91.1$ (Table 1).

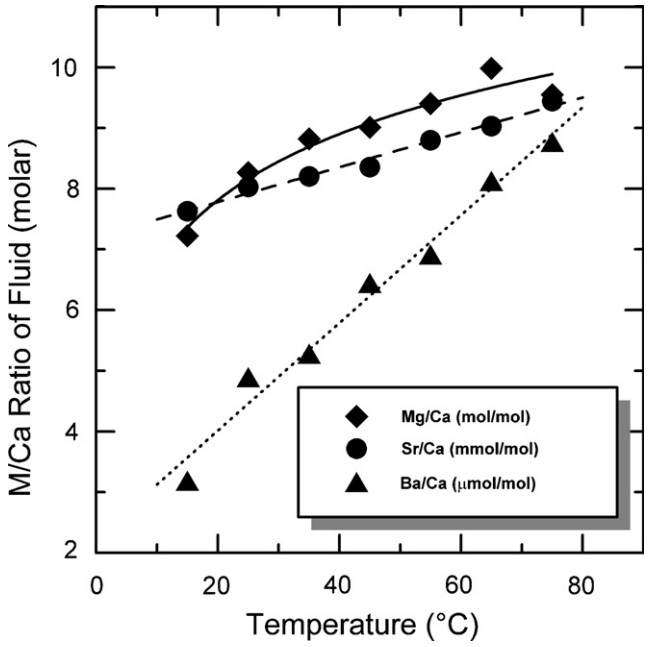

Fig. 1. Relationships between temperature and Ca-normalized molar concentrations of Mg (diamonds, solid curve), Sr (circles, dashed curve), and Ba (triangles, dotted curve) in the final fluids from aragonite precipitation experiments reported in this study.

The Mg/Ca, Sr/Ca, and Ba/Ca ratios of the Vineyard Sound seawater were 5.23 ± 0.02 mol/mol, 8.45 ± 0.04 mmol/mol, and 5.24 ± 0.07 μmol/mol, respectively, at the beginning of each experiment. Following precipitation of calcite the Mg/Ca ratio of the fluid in the experiment carried out at 5 °C was 7.15 ± 0.04 mol/mol, the Sr/Ca ratio was 8.69 ± 0.02 mmol/mol, and the Ba/Ca ratio was 4.50 ± 0.05 μmol/mol. In the experiments that precipitated aragonite, the Mg/Ca ratios of the fluids increase from 7.22 ± 0.02 mol/mol at 15 °C to

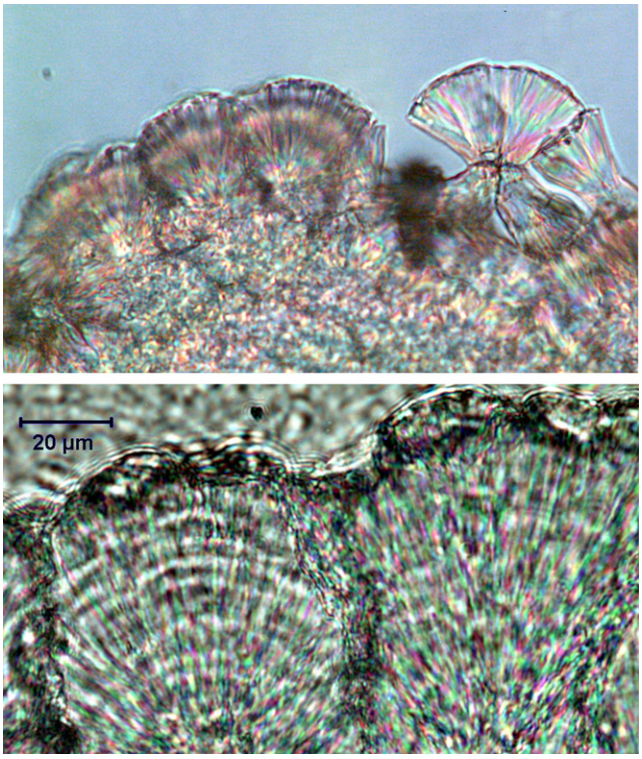

Fig. 2. Transmitted-light photomicrographs comparing aragonite grains precipitated experimentally at 45 °C in experiment ASW-3 (top) with aragonite from the thecal wall of the corallite of *L. pertusa* collected in 2003 at 129 m depth on the Tisler Reef, NE Skagerrak (bottom) (Cohen et al., 2006). Scale bar is 20 μm.

Table 3
Elemental ratios in experimentally precipitated calcite and aragonite

Experiment	*n*	Mg/Ca	Sr/Ca	Ba/Ca	Ca
ASW-6	7	84.4(15)	3.15(1)	9.97(14)	37.1(6)[a]
ASW-4	10	9.9(15)	9.85(17)	14.2(7)[b]	
ASW-1	10	8.5(5)	9.43(7)	13.8(3)[c]	39.62(11)
ASW-2	9	7.4(8)	9.17(13)	10.5(15)	39.51(10)[a]
ASW-3	10	6.3(7)	8.99(13)	8.5(5)	39.42(11)
ASW-7	10	5.1(8)	8.00(17)	5.0(4)	
ASW-8	10	4.2(6)	7.99(16)	4.6(5)	
ASW-9	10	3.6(5)	7.7(3)	4.3(5)	

Notes: *n* is the number of analyses included in the reported mean. Mg/Ca and Sr/Ca ratios are reported in mmol/mol; Ba/Ca ratios are reported in μmol/mol; Ca is reported in weight percent. Units in parentheses represent 1 standard error in terms of least units cited, on the basis of replicate analyses. Therefore, 84.4(15) should be read as 84.4 ± 1.5.
[a] Ten points included in mean.
[b] Sixteen points included in mean.
[c] Eleven points included in mean.

9.55 ± 0.04 mol/mol at 75 °C, while the Sr/Ca ratio increases from 7.63 ± 0.02 to 9.44 ± 0.03 mmol/mol and Ba/Ca ratio increases from 3.19 ± 0.04 to 8.77 ± 0.07 μmol/mol (Fig. 1).

The carbonate grains that precipitated in all of the experiments are spherulitic (Fig. 2). The calcite grains are ~30–60 μm in diameter, while the aragonite grains range from ~30 to ~150 μm in diameter. The calcite contains 37.1 ± 0.6 wt% Ca, and has Mg/Ca, Sr/Ca, and Ba/Ca ratios of 84.4 ± 1.5, 3.15 ± 0.1 mmol/mol, and 9.97 ± 0.14 μmol/mol, respectively (Table 3). The Ca contents of aragonite that precipitated in the experiments carried out at 25, 35, and 45 °C are indistinguishable from one another, with a mean value of 39.52 ± 0.10 wt% (Table 3). The Mg/Ca ratio of the experimentally precipitated aragonite decreases by 64% between 15 and 75 °C, from 9.9 ± 1.5 to 3.6 ± 0.5 mmol/mol (Fig. 3a). This decrease is described by the following relationship:

$$\ln \frac{\mathrm{Mg}}{\mathrm{Ca}} = \frac{1747 \pm 94}{T} - 3.7 \pm 0.3, \tag{1}$$

where Mg/Ca is in mmol/mol and T is in Kelvin (solid curve in Fig. 3a). The square of the correlation coefficient (r^2) for the fit is 0.986. The Sr/Ca ratio of the aragonite precipitated in our experiments decreases by 20% between 15 and 75 °C, from 9.85 ± 0.17 to 7.7 ± 0.3 mmol/mol (Fig. 3a), according to the equation:

$$\ln \frac{\mathrm{Sr}}{\mathrm{Ca}} = \frac{435 \pm 48}{T} + 0.79 \pm 0.15, \tag{2}$$

where Sr/Ca is in mmol/mol and T is in Kelvin (dashed curve in Fig. 3a). The square of the correlation coefficient for the fit is 0.942. If our data are fit using a linear relationship between Sr/Ca and temperature, the result is nearly identical to that derived by Smith et al. (1979) using the Doerner–Hoskins Sr/Ca exchange coefficient ($K_{\mathrm{DH}}^{\mathrm{Sr/Ca}}$) versus temperature regression of Kinsman and Holland (1969) and an assumed Sr/Ca ratio for the fluid of 8.6 mmol/mol. The Ba/Ca ratio of the experimentally precipitated aragonite decreases by ~70% between 15 and 75 °C, from 14.2 ± 0.7 to 4.3 ± 0.5 μmol/mol (Fig. 3b) according to the following relationship:

$$\ln \frac{\mathrm{Ba}}{\mathrm{Ca}} = \frac{2337 \pm 270}{T} - 5.3 \pm 0.9, \tag{3}$$

where Ba/Ca is in μmol/mol and T is in Kelvin (dotted curve in Fig. 3b). The square of the correlation coefficient for the fit is 0.937.

4. Discussion

4.1. Partitioning of Mg^{2+}, Ca^{2+}, Sr^{2+}, and Ba^{2+} between aragonite and seawater

At thermodynamic equilibrium the distribution of a minor component, such as Sr^{2+}, between aragonite and fluid can be described by an exchange reaction of the form:

$$\mathrm{Ca}^{\mathrm{Aragonite}} + \mathrm{Sr}^{\mathrm{Fluid}} = \mathrm{Sr}^{\mathrm{Aragonite}} + \mathrm{Ca}^{\mathrm{Fluid}}. \tag{4}$$

The temperature and compositional dependencies of this equilibrium are given by:

$$\ln K_{\mathrm{D}}^{\mathrm{Sr/Ca}} = \ln \frac{X_{\mathrm{Sr}}^{\mathrm{Aragonite}} X_{\mathrm{Ca}}^{\mathrm{Fluid}}}{X_{\mathrm{Ca}}^{\mathrm{Aragonite}} X_{\mathrm{Sr}}^{\mathrm{Fluid}}} = -\frac{\Delta H^0}{RT} + \frac{\Delta S^0}{R} - \ln \frac{\gamma_{\mathrm{Sr}}^{\mathrm{Aragonite}} \gamma_{\mathrm{Ca}}^{\mathrm{Fluid}}}{\gamma_{\mathrm{Ca}}^{\mathrm{Aragonite}} \gamma_{\mathrm{Sr}}^{\mathrm{Fluid}}}, \tag{5}$$

where X is mole fraction, ΔH^0, and ΔS^0 are, respectively, the standard state enthalpy and entropy changes associated with the exchange reaction, R is the gas constant, T is temperature in Kelvin, and γ is an activity coefficient (e.g., Denbigh, 1981). During closed system precipitation of aragonite from seawater at low temperatures, grain interiors do not maintain equilibrium with the evolving composition of the fluid because diffusion in the crystal is not efficient enough to maintain its homogeneity. The result is a continuously zoned aragonite grain. At these conditions, Eq. (5) is valid only for the outer portion of the growing crystal; distribution of the minor component between the final fluid and a coexisting aragonite grain is described by the Doerner–Hoskins relationship:

$$\log\left(1 + \frac{m_{\mathrm{Sr}}^{\mathrm{Aragonite}}}{m_{\mathrm{Sr}}^{\mathrm{Fluid}}}\right) = K_{\mathrm{DH}}^{\mathrm{Sr/Ca}} \log\left(1 + \frac{m_{\mathrm{Ca}}^{\mathrm{Aragonite}}}{m_{\mathrm{Ca}}^{\mathrm{Fluid}}}\right), \tag{6}$$

where $m_i^{\mathrm{Aragonite}}$ is the total number of moles of Sr or Ca in the final precipitate, and m_i^{Fluid} is the total number of moles of Sr or Ca in the final fluid (Doerner and Hoskins, 1925). Holland et al. (1963) demonstrated that in a closed system the distribution of Sr^{2+} between experimentally precipitated aragonite and the coexisting fluid is governed by Eq. (6) to temperatures as high as 100 °C. Kinsman and Holland (1969) established experimentally the temperature dependence of $K_{\mathrm{DH}}^{\mathrm{Sr/Ca}}$ at temperatures of 16–80 °C. Zhong and Mucci (1989) and Mucci et al. (1989) precipitated aragonite

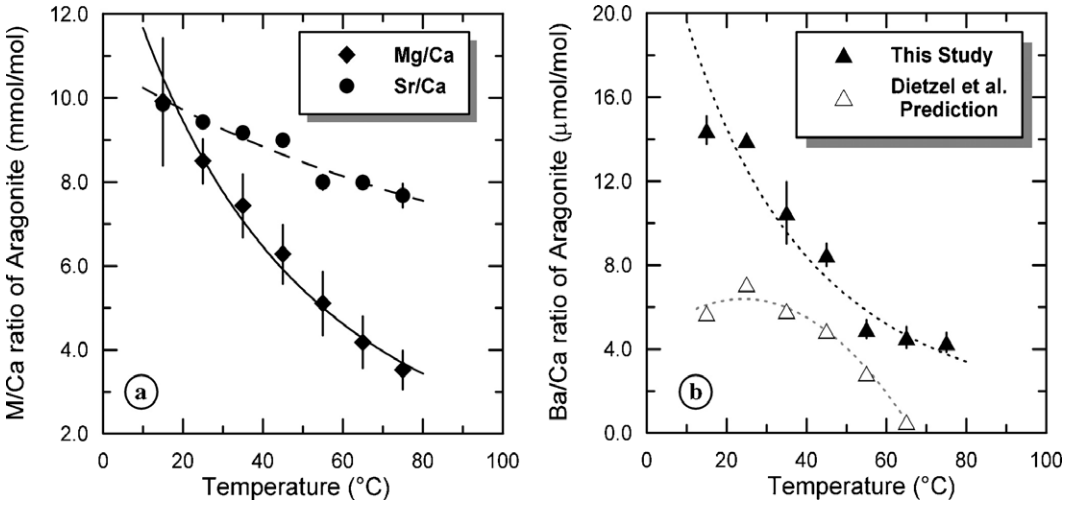

Fig. 3. Relationships between temperature and (a) Mg/Ca (diamonds, solid curve), Sr/Ca (circles, dashed curve), and (b) Ba/Ca ratios (solid triangles, dotted curve) of aragonite precipitated experimentally at 15–75 °C. Open triangles are the Ba/Ca ratios predicted for our experiments using Eq. (6) of Dietzel et al. (2004). Uncertainties are 1 standard error based on replicate analyses.

from seawater experimentally at 25 °C to investigate the influence of salinity and dissolved sulfate, respectively, on precipitation rate and the incorporation of Sr^{2+} into aragonite. Precipitation was carried out while maintaining a nearly constant fluid composition (i.e. in an open system), so that the distribution of Sr follows a homogeneous distribution law ($K_{Eq}^{Sr/Ca}$ in Eq. (5)). Results from these studies indicate that the incorporation of Sr^{2+} into aragonite is independent of variations in both salinity and dissolved sulfate ion concentration.

We used the experimental approach of Kinsman and Holland (1969) to precipitate carbonate from seawater at temperatures of 5 to 75 °C to augment existing data for element distribution in abiogenic systems and, thereby, provide a framework for interpreting the compositions of biogenic carbonates. The experimental results of Kinsman and Holland (1969) have been used extensively over the past 35 years as an abiogenic reference for evaluating the influence of "vital effects," leading to significant advances in our understanding of the factors that control the Sr/Ca ratio of biogenic aragonite (e.g., Smith et al., 1979; de Villiers et al., 1994; Cohen et al., 2002). Experimental data bearing on the distribution of Mg^{2+}, a proxy for sea surface temperature, and of Ba^{2+}, a proxy for oceanic upwelling and coastal river runoff, between abiogenic aragonite and aqueous fluid are sparse. Kitano et al. (1971) reported $K_{DH}^{Ba/Ca}$ values of ~1 for aragonite precipitated from a calcium bicarbonate solution at 20 ± 1 °C. Dietzel et al. (2004) investigated the distribution of Ba^{2+} between aragonite and an aqueous Ca^{2+}–Mg^{2+}–Cl^- solution and reported Ba/Ca distribution coefficients that decrease linearly from 1.91 ± 0.09 at 10 °C to 0.62 ± 0.09 at 50 °C.

Table 4 and Figs. 4–6 summarize the aragonite-fluid Doerner–Hoskins exchange coefficients for Mg^{2+}, Sr^{2+}, and Ba^{2+} ($K_{DH}^{Mg/Ca}$, $K_{DH}^{Sr/Ca}$ and $K_{DH}^{Ba/Ca}$, respectively) determined from our experiments. At 15 °C $K_{DH}^{Ba/Ca}$ (2.99 ± 0.09) is significantly larger than either $K_{DH}^{Sr/Ca}$

Table 4
Doerner–Hoskins exchange coefficients for Mg, Sr, and Ba

Expt	Temperature (°C)	$K_{Mg/Ca}$	$K_{Sr/Ca}$	$K_{Ba/Ca}$
ASW-6	5	0.0149(3)	0.417(4)	1.81(2)
ASW-4	15	0.0017(3)	1.24(2)	2.99(9)
ASW-1	25	0.00133(8)	1.133(8)	2.11(4)
ASW-2	35	0.00104(7)	1.089(12)	1.64(15)
ASW-3	45	0.00091(11)	1.058(12)	1.23(6)
ASW-7	55	0.00074(11)	0.93(2)	0.77(5)
ASW-8	65	0.00059(7)	0.912(14)	0.64(6)
ASW-9	75	0.00053(6)	0.85(2)	0.57(5)

Notes: Units in parentheses represent 1 standard error in terms of least units cited based on propagation of analytical uncertainties. Therefore, 0.0149(3) should be read as 0.0149 ± 0.0003.

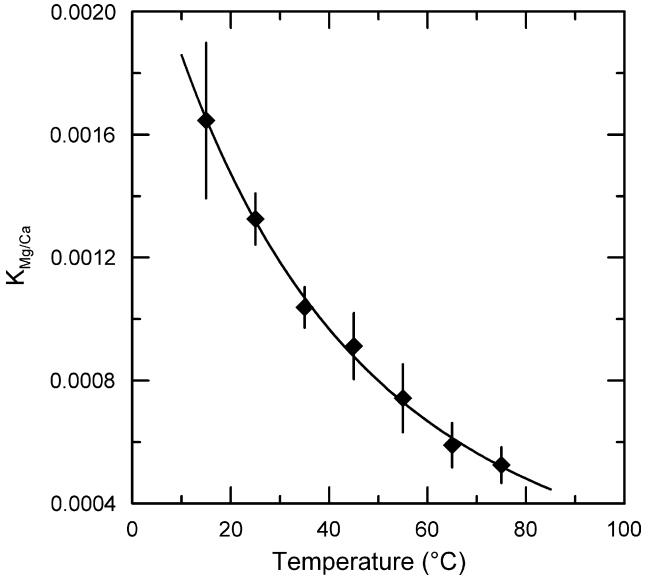

Fig. 4. Temperature dependence of the Doerner–Hoskins Mg/Ca exchange coefficient calculated for our experiments using Eq. (6). Uncertainties are 1σ.

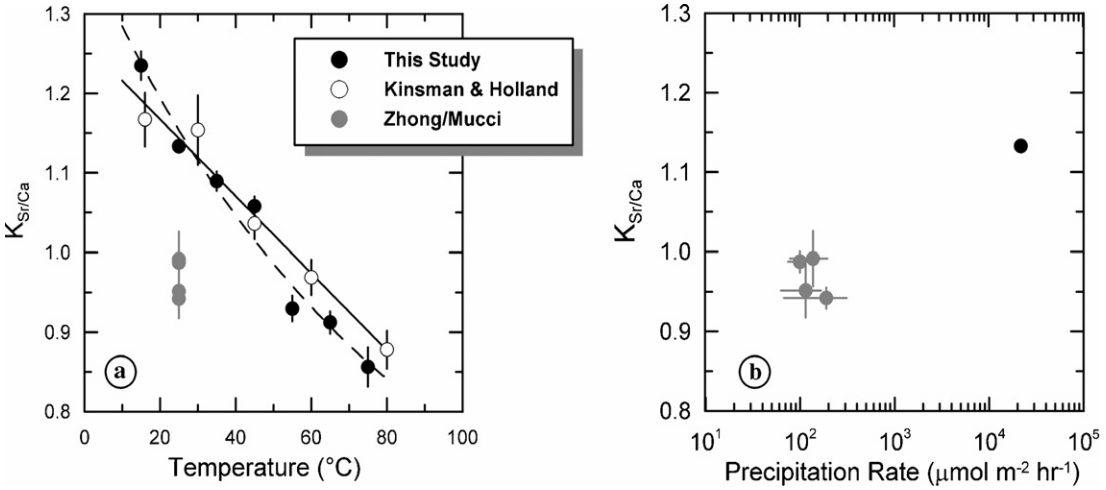

Fig. 5. (a) Comparison of the temperature dependencies of Doerner–Hoskins Sr/Ca exchange coefficients calculated for our experiments (solid circles) with those determined experimentally by Kinsman and Holland (1969) (open circles), Zhong and Mucci (1989), and Mucci et al. (1989) (shaded circles). Solid line represents a linear fit to the data of Kinsman and Holland (1969). Dashed line is a fit of our experimental data to Eq. (8). (b) Precipitation rate dependence of Sr/Ca exchange coefficients at 25 °C showing data from this study (filled circle), Zhong and Mucci (1989) and Mucci et al. (1989) (shaded circles).The precipitation rate for our experiment was estimated on the basis of the Ω value reported in Table 1 using Eq. (A1.2). Uncertainties are 1σ.

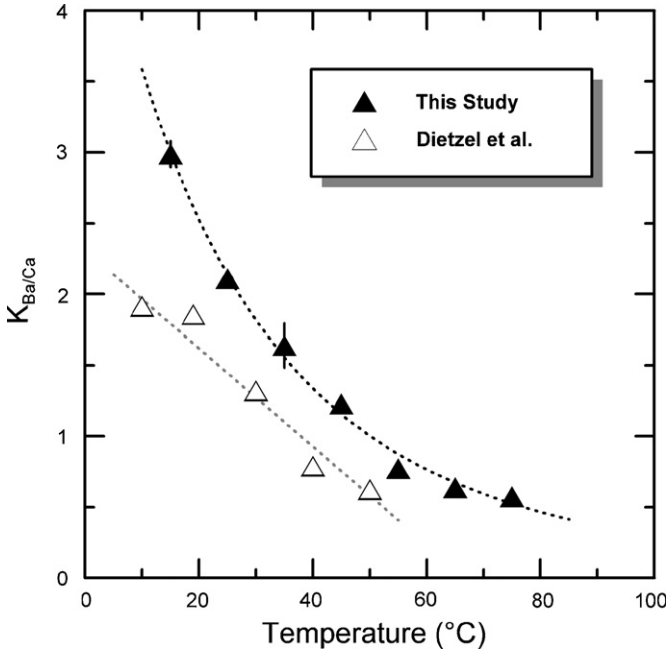

Fig. 6. Comparison of the temperature dependencies of the Doerner–Hoskins Ba/Ca exchange coefficient calculated for our experiments (solid triangles) and those Dietzel et al. (2004) (open triangles). Uncertainties are 1σ.

(1.24 ± 0.02) or $K_{DH}^{Mg/Ca}$ (0.0017 ± 0.0003), demonstrating that Ba^{2+} is more compatible in aragonite at these conditions than either Sr^{2+} or Mg^{2+}. Exchange coefficients for all three elements decrease monotonically with increasing temperature. The strongest temperature dependence is associated with $K_{DH}^{Ba/Ca}$, which decreases by 81% between 15 and 75 °C; $K_{DH}^{Mg/Ca}$ decreases by 69% and $K_{DH}^{Sr/Ca}$ by only 31% over this temperature range. Due to these differing temperature sensitivities, Sr^{2+} $(K_{DH}^{Sr/Ca} = 0.85 \pm 0.02)$ is more compatible in aragonite precipitated at 75 °C than either Ba^{2+} $(K_{DH}^{Ba/Ca} = 0.57 \pm 0.05)$ or Mg^{2+} $(K_{DH}^{Mg/Ca} = 0.00053 \pm 0.00006)$. The temperature dependencies of the Doerner–Hoskins exchange coefficients are governed by the following equations:

$$\ln K_{DH}^{Mg/Ca} = \frac{1930 \pm 55}{T} - 13.1 \pm 0.2, \quad (7)$$

$$\ln K_{DH}^{Sr/Ca} = \frac{605 \pm 47}{T} - 1.89 \pm 0.15, \quad (8)$$

$$\ln K_{DH}^{Ba/Ca} = \frac{2913 \pm 154}{T} - 9.0 \pm 0.5, \quad (9)$$

where T is in Kelvin. The square of the correlation coefficients (r^2) for the fits represented by Eqs. (7)–(9) are 0.996, 0.971, and 0.986, respectively.

Fig. 5a compares $K_{DH}^{Sr/Ca}$ values from this study with those of Kinsman and Holland (1969) (open symbols), and the $K_D^{Ba/Ca}$ values of Mucci et al. (1989) and Zhong and Mucci (1989) (gray symbols). There is very good agreement between our experimental results and those of Kinsman and Holland (1969), although the latter define a marginally weaker temperature dependence (solid line in Fig. 5a). The $K_D^{Sr/Ca}$ values determined at 25 °C by Mucci et al. (1989) and Zhong and Mucci (1989) are systematically low by ~15% relative to the other data. The mean $K_{Eq}^{Sr/Ca}$ of 0.97 ± 0.01 for the aragonite from these experiments corresponds with a precipitation temperature of ~61 °C according to a linear regression of the Kinsman and Holland (1969) data, and of ~53 °C on the basis of Eq. (8). This offset is consistent with the existence of a precipitation rate dependence for the incorporation of Sr^{2+} into aragonite (Fig. 5b). The initial Ω with respect to aragonite for our 25 °C experiment was 46.7 (Table 1), which corresponds to a precipitation rate of $\sim 2 \times 10^4$ μmol m^{-2} h^{-1} according to the data of Burton and Walter (1987) [Eq. (A1.2) in

Appendix A]. The mean precipitation rate for the experiments in the combined studies of Zhong and Mucci (1989) and Mucci et al. (1989) was only 130 μmol m^{-2} h^{-1}. Therefore, it is probable that a precipitation rate dependence exists for the incorporation of Sr^{2+} into aragonite. That no precipitation rate dependence was identified in the studies of Kinsman and Holland (1969), Zhong and Mucci (1989) or Mucci et al. (1989) may reflect the relatively narrow range of precipitation rates investigated by individual studies. The probable existence of a precipitation rate dependence is an indication that kinetics influence the incorporation of Sr^{2+} into abiogenic aragonite.

4.2. Determination of equilibrium partitioning from lattice strain theory

The role of kinetics in controlling experimentally determined partition coefficients can be evaluated by comparing experimental data with an independent estimate for the equilibrium state (e.g., Rimstidt et al., 1998; Wang and Xu, 2001). Here, we briefly review the lattice-strain approach to modeling element partitioning, and use it to predict the equilibrium partitioning of Mg^{2+}, Sr^{2+}, and Ba^{2+} between aragonite and seawater at the conditions of our experiments. Comparisons of our experimental data (Tables 4 and 5) with predictions from both the lattice strain model and equilibrium thermodynamics demonstrate that kinetics plays a major role in determining the composition of abiogenic aragonite. Further, we show that surface entrapment is the process most likely to be controlling the composition of our experimentally precipitated aragonite, and that the temperature dependencies discussed in the previous section are consistent with temperature-driven changes in diffusivity in the near-surface region of growing crystals.

The partitioning of a minor or trace component i between a crystal and coexisting aqueous fluid or silicate melt is described by the Nernst partition coefficient:

$$D_i^{\text{Mineral/Fluid}} = \frac{X_i^{\text{Mineral}}}{X_i^{\text{Fluid}}}, \tag{10}$$

Table 5
Nernst partition coefficients for Mg, Ca, Sr, and Ba

Expt	Temperature (°C)	D_{Mg}	D_{Ca}	D_{Sr}	D_{Ba}
ASW-6	5	21.7(4)	1840(13)	667(5)	4075(73)
ASW-4	15	2.7(4)	1961(6)	2533(45)	8701(419)
ASW-1	25	2.37(15)	2307(8)	2709(22)	6598(172)
ASW-2	35	1.86(12)	2366(7)	2645(38)	4705(660)
ASW-3	45	1.7(2)	2385(13)	2567(37)	3136(195)
ASW-7	55	1.3(2)	2459(13)	2235(49)	1766(156)
ASW-8	65	1.07(13)	2558(7)	2263(45)	1436(153)
ASW-9	75	0.86(9)	2303(8)	1874(69)	1135(14)

Notes: Partition coefficients are reported in weight units. Units in parentheses represent 1 standard error uncertainties in terms of least units cited, calculated by propagating analytical uncertainties. Therefore, 21.7(4) should be read as 21.7 ± 0.4.

where X is mole fraction; for convenience weight concentration is often substituted for mole fraction. At equilibrium the Nernst partition coefficients for trace elements of a given valence state substituting onto a single lattice site vary systematically as a function of cationic radius (Onuma et al., 1968). This variability results from the contribution of strain energy, due to the misfit between a substituent cation and the lattice site, to the free energy change for incorporating a cation that fits exactly onto the site (Nagasawa, 1966; Brice, 1975; Beattie, 1994; Blundy and Wood, 1994). As the misfit between the optimum radius for the lattice site (r_0) and the radius of the substituent cation (r_i) increases, the Nernst partition coefficient decreases according to the equation:

$$D_i^{\text{Mineral/Fluid}} = D_0 \exp\left(\frac{-4\pi E N_A \left(\frac{r_0}{2}(r_i - r_0)^2 + \frac{1}{3}(r_i - r_0)^3\right)}{RT}\right), \tag{11}$$

where D_0 is the mineral/fluid partition coefficient for the strain-free substitution, E is the effective Young's Modulus for the lattice site, N_A is Avogadro's number, R is the gas constant, and T is temperature in Kelvin (Brice, 1975; Blundy and Wood, 1994; Wood and Blundy, 1997).

In experimental studies of high temperature systems the lattice strain equation is typically used as a functional form for fitting experimentally determined trace element partition coefficients. The derived values for D_0, E, and r_0 are then either parameterized to derive predictive models that can be applied to natural systems or used to extrapolate available data to predict partition coefficients for cations that have not been investigated experimentally (e.g., Wood and Blundy, 1997). We used Eq. (11) to perform a forward calculation to predict (metastable) equilibrium element partitioning between aragonite and seawater, providing a baseline for evaluating the role of kinetics in controlling the element distributions measured in our low-temperature experiments. These calculations rely on several approximations. First, we assumed that the effective Young's Modulus (E) for the 9-coordinated aragonite lattice site is equal to the 92 GPa Young's modulus for the bulk crystal (Bass, 1995). Blundy and Wood (1994) have shown this to be a valid approximation for isovalent substitutions. The optimum radius (r_0) was taken to be 1.18 Å, on the basis of the cationic radius for 9-coordinated Ca^{2+} (Shannon, 1976). This is within the range of r_0 values that are consistent with a mean metal-oxygen distance of 2.528 ± 0.085 Å for the 9-coordinated aragonite lattice site and an ionic radius of 1.42 Å for O^{2-} (Shannon, 1976; Smyth and Bish, 1988). Finally, D_0 was set equal to our experimentally determined value for $D_{Ca}^{\text{Aragonite/Seawater}}$ at a given temperature. As the essential structural constituent of aragonite, Ca^{2+} represents the most likely strain-free "substitution."

Results from these calculations (open circles) are compared with our experimentally determined $K_{DH}^{Sr/Ca}$ values (filled circles) in Fig. 7. Also shown (open squares)

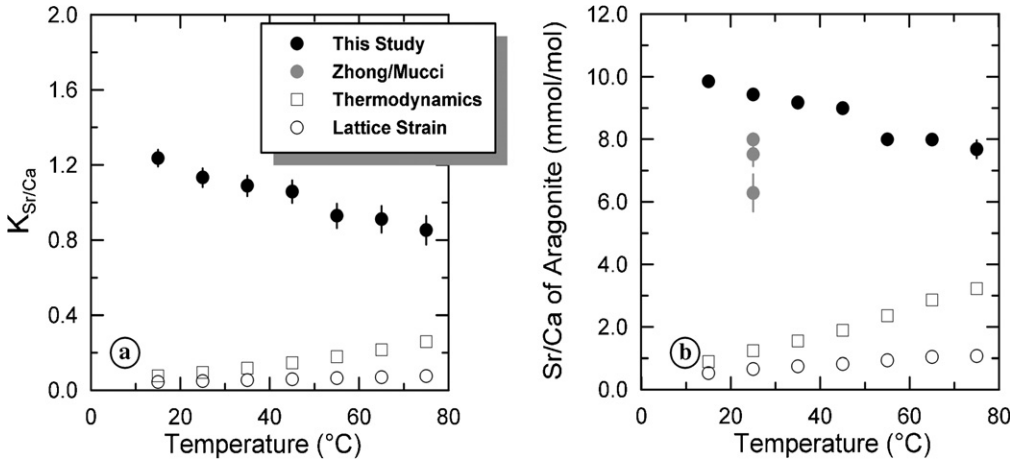

Fig. 7. (a) Comparison of experimentally determined Doerner–Hoskins Sr/Ca exchange coefficient from this study (solid circles) with equilibrium exchange coefficients calculated from thermodynamics (open squares) and the lattice strain equation (open circles). (b) Comparison of Sr/Ca ratios of experimentally precipitated aragonite from this study (solid circles) and those of Zhong and Mucci (1989), and Mucci et al. (1989) (shaded circles) with equilibrium aragonite compositions calculated from thermodynamics (open squares) and the lattice strain equation (open circles). All uncertainties are 1σ.

are results from calculations of the Sr/Ca exchange coefficient between aragonite and seawater:

$$K^{Sr/Ca} = \frac{K_{Aragonite}}{K_{Strontianite}} \cdot \frac{\lambda_{CaCO_3}}{\lambda_{SrCO_3}} \cdot \frac{\gamma_{Sr^{2+}}}{\gamma_{Ca^{2+}}}, \quad (12)$$

where K_i are equilibrium constants for aragonite and strontianite, λ_i are activity coefficients for $CaCO_3$ and $SrCO_3$ components in aragonite, and γ_i are activity coefficients for Sr^{2+} and Ca^{2+} cations in seawater. These calculations were carried out using the thermochemical data compiled by Nordstrom et al. (1990), activity coefficients for $CaCO_3$ and $SrCO_3$ components in aragonite determined experimentally by Plummer and Busenberg (1987) and the assumption that the activity coefficient for Sr^{2+} in seawater is equal to that for Ca^{2+} (i.e., $\gamma_{Sr^{2+}}/\gamma_{Ca^{2+}} = 1$). There are several important differences between the results from experiments and calculations that suggest the former (and by inference the experimental results from previous aragonite precipitation studies) do not represent a close approach to equilibrium. First, there is good agreement between the Sr/Ca exchange coefficients predicted from equilibrium thermodynamics and those calculated using the lattice strain equation. That the former are systematically larger may be an indication that $\gamma_{Sr^{2+}}/\gamma_{Ca^{2+}}$ is less than unity; allowing this activity coefficient ratio to vary from 0.58 at 15 °C to 0.30 at 75 °C brings the two sets of calculations into agreement. Second, the experimentally determined $K_{DH}^{Sr/Ca}$ values are ~10–30 times larger than the equilibrium exchange coefficients predicted from equilibrium thermodynamics and the lattice strain calculations. Finally, both equilibrium thermodynamics and the lattice strain calculations predict positive temperature dependencies for the Sr/Ca exchange coefficient, whereas the experimentally determined values decrease systematically with increasing temperature. Note that while the enthalpy change associated with the substitution of Sr^{2+} for Ca^{2+} in aragonite is positive, producing a negative temperature dependence for the equilibrium constant, the positive temperature dependence of the exchange coefficient is dominated by the increase in $\lambda_{CaCO_3}/\lambda_{SrCO_3}$ from 0.0078 at 15°C to 0.0430 at 75 °C. Therefore, the equilibrium Sr/Ca ratio of abiogenic aragonite precipitated from seawater should *increase* from ~0.51 mmol/mol at 15 °C to ~1.00 mmol/mol at 75 °C rather than decreasing from 9.85 ± 0.17 to 7.7 ± 0.3 mmol/mol (Fig. 7b).

Aragonite–seawater partition coefficients predicted at 15 and 75 °C using Eq. (11) are compared with the results from our experiments in Fig. 8. The partitioning of Mg^{2+}, Sr^{2+}, and Ba^{2+} between aragonite and seawater in the experiment performed at 15 °C defines a linear relationship between $\log D_i^{Aragonite/Fluid}$ and cationic radius (dotted line in Fig. 8a), rather than conforming to the parabolic relationship predicted by the lattice strain (solid curve in Fig. 8a). The relationship between $\log D_i^{Aragonite/Fluid}$ and cationic radius becomes increasingly parabolic in experiments performed at progressively higher temperatures until, at 75 °C, the partitioning of Mg^{2+}, Sr^{2+}, and Ba^{2+} between aragonite and seawater conforms to Eq. (11) (Fig. 8b). However, the effective Young's modulus of 26 GPa derived from a fit of the data from this experiment is significantly smaller than that of aragonite (92 GPa), and the optimum radius (1.36 Å) is comparable to that of 9-coordinated Sr^{2+} (1.31 Å) rather than 9-coordinated Ca^{2+} (1.18 Å) (Shannon, 1976). The systematic discrepancies between the predicted equilibrium partition coefficients and the experimentally determined values indicate that the aragonite precipitated in each of our experiments is strongly enriched in trace components (''impurities'') relative to the concentrations expected from equilibrium partitioning between fluid and the growing crystals.

There are several kinetic mechanisms capable of producing impurity enrichments. If cation transport in the fluid is too slow to replenish components preferentially incorporated into the lattice, a compositionally distinct boundary

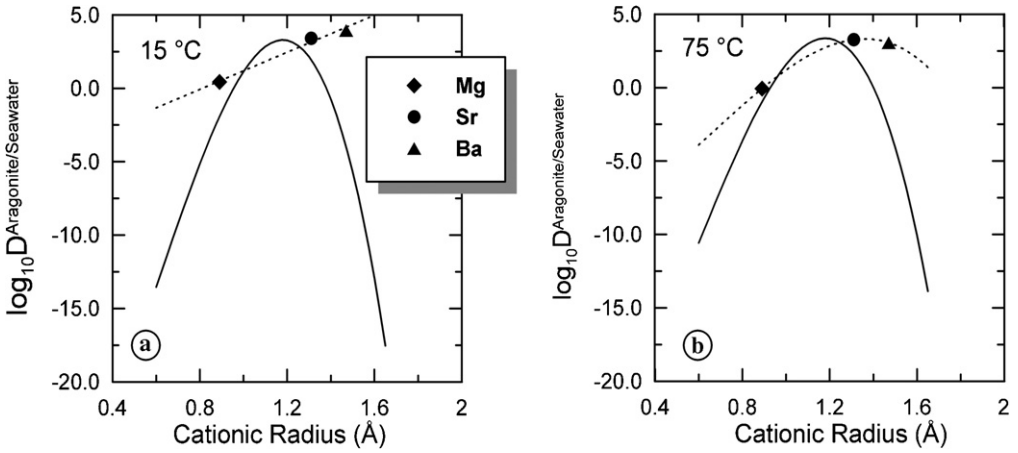

Fig. 8. Comparison of experimentally determined aragonite–seawater partition coefficients for Mg^{2+} (diamonds), Sr^{2+} (circles), and Ba^{2+} (triangles) with equilibrium partitioning calculated from the lattice strain equation (solid curve) at (a) 15 °C and (b) 75 °C. Dotted curves are fits to the experimental data. All uncertainties are 1σ.

layer develops in the fluid adjacent to the growing crystal. A narrow zone at the fluid–mineral interface becomes depleted in elements that are compatible in the crystal, and enriched in elements that are excluded (e.g., Tiller et al., 1953). While the existence of a fluid boundary layer will produce impurity enrichments in the precipitate, they are limited to incompatible elements. Because compatible elements are readily incorporated into the growing crystal, they become depleted in the fluid boundary layer and will be similarly depleted, rather than enriched, in the solid. In simple terms: development of a fluid boundary layer shifts all experimentally determined partition coefficients toward unity. The predicted equilibrium aragonite–seawater partitioning of Mg^{2+}, Sr^{2+}, and Ba^{2+} ranges from compatible ($D_{Sr}^{Aragonite/Seawater} = 65$ to 137) to strongly incompatible ($D_{Mg}^{Aragonite/Seawater} = 0.01$ to 0.11; $D_{Ba}^{Aragonite/Seawater} = 2.0 \times 10^{-5}$ to 5.5×10^{-5}). Given that all of these elements are enriched in the experimentally precipitated aragonite, development of a fluid boundary layer cannot explain our experimental data.

A second mechanism for producing impurity enrichments is growth of a crystal from a finite fluid reservoir under conditions where lattice diffusion is not rapid enough to maintain equilibrium between the interior of the crystal and the evolving composition of the fluid. This produces a continuously zoned crystal, and can be accounted for when calculating exchange coefficients through the Doerner–Hoskins relationship (sometimes referred to as logarithmic distribution law). Partition coefficients calculated from the compositions of the average solid and the final fluid will be a function of the mass fraction of solid precipitated, and will diverge from unity relative to equilibrium values. Incompatible elements will be depleted in the resulting crystal relative to equilibrium, while compatible elements are enriched (Albarede and Bottinga, 1972). Although the aragonite grains precipitated in our experiments are almost certainly zoned, the observation that both compatible and incompatible elements are enriched in our experimentally precipitated aragonite indicates that this is a secondary effect, and precludes this mechanism as an explanation for our data.

A third mechanism for producing impurity enrichments involves partial equilibration and entrapment of the near-surface region during crystal growth (Watson and Liang, 1995; Watson, 1996, 2004). The equilibrium concentration of a given element is likely to vary continuously in the near-surface region of a crystal, owing to the fact that it is structurally distinct from the regular lattice (e.g., Hiraga et al., 2004). These compositional gradients can produce either enrichments or depletions of specific elements in the near-surface region relative to the bulk crystal. As the near-surface region is incorporated into the lattice during crystal growth, its composition must be modified by solid-state diffusion (or some other transport mechanism) in order for equilibrium to be maintained. At conditions where crystal growth rate is rapid relative to cation transport in the near surface region, such as at low temperatures, the inefficiency of this transformation process is capable of producing significant enrichments and/or depletions in minor or trace elements relative to equilibrium. This process has been proposed by Watson (1996, 2004) as an explanation for both sector zoning and the precipitation-rate dependence of element partitioning during the growth of calcite from aqueous fluid. Below we present results from finite-difference calculations that demonstrate the capacity of surface entrapment to produce the compositional variations in our experimentally precipitated aragonite. Decreases in the Mg/Ca, Sr/Ca, and Ba/Ca ratios of the experimental aragonite with increasing temperature likely reflect a systematic increase in the efficiency of the surface-to-volume transformation process as solid-state transport rates increase.

4.3. Surface entrapment control on the composition of abiogenic aragonite

The comparison, presented above, of our experimentally determined aragonite–seawater partition coefficients to

equilibrium values predicted using the lattice strain equation of Blundy and Wood (1994) indicates significant enrichments in Mg^{2+}, Sr^{2+}, and Ba^{2+}. These enrichments are independent of whether the predicted equilibrium partition coefficients are greater than or less than unity, and they decrease with increasing temperature. These observations are consistent with surface entrapment, a kinetic process thought to operate in regimes where the competition between crystal growth rate and diffusivity in the near-surface region limits the extent to which the solid can achieve partitioning equilibrium with the fluid (Watson and Liang, 1995; Watson, 1996, 2004). Here, we present results from calculations carried out using the finite difference model of Watson and Liang (1995), with the modifications of Watson (2004), that demonstrate the capacity of surface entrapment to produce the compositional variations observed in our experimentally precipitated aragonite.

Quantitative modeling of surface entrapment requires knowledge of (1) the width of the compositionally distinct near-surface region ($2l$), (2) the form of the concentration versus distance profile for the element of interest in the near-surface region ($C_i(x)$), (3) the growth rate of the crystal (V), (4) lattice diffusivity for the cation of interest ($\mathcal{D}_B$), (5) the surface enrichment factor, or the concentration at the surface relative to the crystal interior, (F) and (5) diffusivity in the near surface region ($\mathcal{D}_S$). Values for l, $C_i(x)$, V and $\mathcal{D}_B$ were estimated as described in Appendix A. The variables F and $\mathcal{D}_S$ were treated as unknowns in our calculations, and solved for by requiring that the temperature dependence of $\mathcal{D}_S$ conform to an Arrhenius law.

Calculations were carried out as follows. First, enrichments were calculated for Mg, Sr, and Ba in each experiment by dividing the experimentally determined partition coefficient by the equilibrium value derived from the lattice strain equation. As a starting point for the first set of calculations, F values were set equal to the largest experimentally determined enrichments (i.e. those at 15 °C). Calculations were then carried out to determine the $\mathcal{D}_S$ value required to reproduce the experimentally determined enrichment for each element. Once $\mathcal{D}_S$ values had been determined for each experiment, the fit to an Arrhenius relationship was evaluated and a new series of calculations were carried out for a larger value of F. This process was continued until increasing F resulted in no significant improvement in the fit to an Arrhenius relationship. The results from these calculations are

$$\ln \mathcal{D}_S^{Mg} = \frac{-18400 \pm 900}{T} + 60 \pm 3, \quad (13)$$

$$\ln \mathcal{D}_S^{Sr} = \frac{-9700 \pm 700}{T} + 31 \pm 2, \quad (14)$$

$$\ln \mathcal{D}_S^{Ba} = \frac{-15000 \pm 1000}{T} + 48 \pm 3, \quad (15)$$

where T is in Kelvin and diffusivity is in nm^2/s (Fig. 9). The square of the correlation coefficients (r^2) for the fits represented by Eqs. (13)–(15) are 0.989, 0.976, and 0.975, respectively. The F values determined for Mg, Sr, and Ba in this way are 300, 45, and 1.5×10^8. The F value for Ba is unexpectedly large, and may reflect uncertainty in the cationic radius of Ba^{2+} in the near-surface environment. For example, assuming cationic radii for Ba^{2+} in the near-surface region of 1.35 Å (6-coordination) to 1.42 Å (8-coordination) result in enrichments of ranging from 10^3 to 3.3×10^5 at 15 °C as compared with a value of 8.5×10^7 for 9-coordinated Ba^{2+} (1.47 Å).

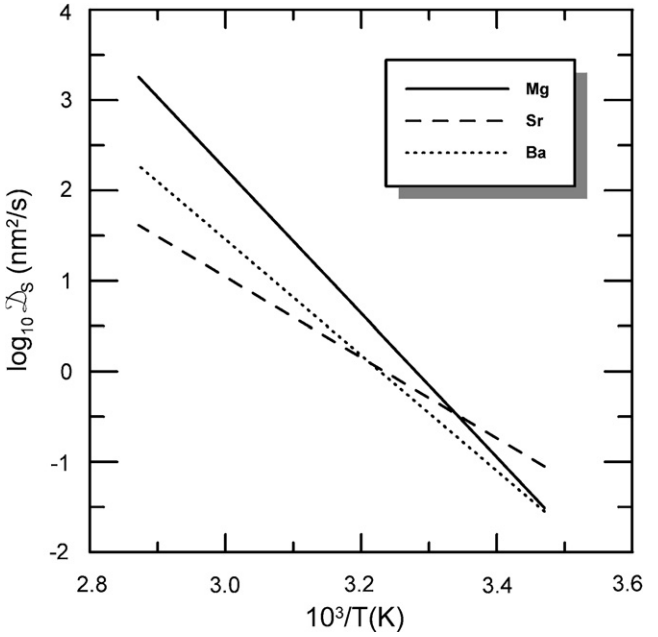

Fig. 9. Arrhenius plot showing diffusivities for Mg^{2+} (solid line), Sr^{2+} (dashed line), and Ba^{2+} (dotted line) in the near-surface region of aragonite inferred from the finite difference calculations described in the text.

The results from surface entrapment calculations carried out using the near-surface Arrhenius laws given by Eqs. (13)–(15) (open symbols) and the F values discussed above are compared with results from our experiments (filled symbols) in Fig. 10. From this comparison it can be seen that surface entrapment is capable of producing the compositional trends observed in our experiments through temperature-driven changes in the rates of cation transport. However, it is important to note that this requires cation transport in the near surface region that is significantly faster than would be expected on the basis of down-temperature extrapolation of high-temperature lattice diffusivities. A similar conclusion was drawn by both Stoll et al. (2002) and Watson (2004) on the basis of comparisons of the surface entrapment model with partitioning data for calcite. Watson (2004) reviewed existing evidence relating to rapid diffusion or high cation mobility in the near-surface region of calcite and found it to be equivocal. While there are no measurements of the lattice diffusivity of Sr in aragonite, a comparison of the near-surface diffusivity implied by Eq. (14) with a down-temperature extrapolation of the lattice diffusivity of Sr in calcite determined by Cherniak (1997) suggests differences of ~16–18 orders of magnitude. If

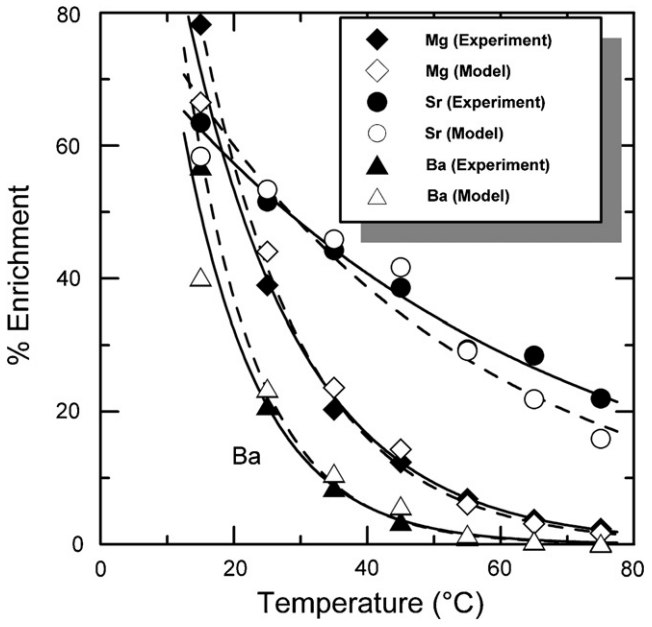

Fig. 10. Comparison of temperature dependencies of lattice enrichments for experimentally precipitated aragonite (filled symbols, solid curve) with results from finite difference calculations (open symbols, dashed curve). Following Watson and Liang (1995), % enrichment is calculated as $100 \times (C(x)_i/C_{oi} - 1)/(F - 1)$, where $C(x)_i$ is the concentration of element i at some distance x from the surface, C_{oi} is the concentration assuming equilibrium partitioning between solid and fluid at infinite distance from the surface, F is the surface enrichment factor.

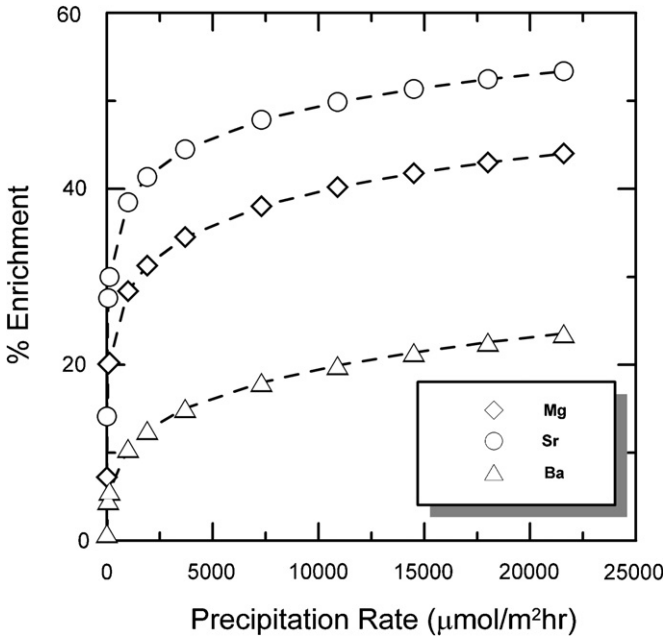

Fig. 11. Precipitation rate dependencies for lattice enrichment of Mg, Sr, and Ba in aragonite at 25 °C predicted from the results of finite difference calculations using Arrhenius relationships given by Eqs. (13)–(15) and shown in Fig. 9.

grain boundary diffusivity is used as a rough guide to cation mobility in the near-surface region, results from experimental studies suggest a difference of ~4–6 orders of magnitude (e.g., Joesten, 1991). However, this comparison is based on high temperature data and relative differences in the activation energies for grain boundary versus lattice diffusivities or changes in the diffusion mechanism are capable of producing significantly larger differences at low temperatures. For example, down-temperature extrapolation of volume and grain boundary diffusivities for Ca^{2+} in calcite determined at 700–900 °C indicates differences of ~18–22 orders of magnitude at the temperatures of our experiments. Therefore, the possibility that near surface transport rates in growing aragonite crystals are ~16–18 orders of magnitude faster than extrapolated lattice diffusivities cannot be ruled out.

There are several ways in which the proposed model can be tested. First, an experimental determination of cation transport rates for both the lattice and the near-surface region of aragonite are needed. These measurements would provide direct constraints on the efficiency of the surface entrapment process during growth of carbonates. A second test is an experimental investigation of the growth rate dependence of element partitioning during precipitation of aragonite from seawater. Precipitation rate dependences for partitioning of Mg^{2+}, Sr^{2+}, and Ba^{2+} into aragonite at 25 °C predicted using the parameters derived from our experiments are shown in Fig. 11. An experimental demonstration that surface entrapment explains both temperature and precipitation rate effects would be an important step in advancing our understanding of kinetic controls on the composition of both abiogenic and biogenic aragonite.

4.4. Comparison of biogenic and experimentally precipitated aragonite

As noted in the introduction, paleoceanographic reconstructions are typically derived from biogenic carbonates using empirical relationships between elemental ratios and environmental variables calibrated using the skeletons of organisms grown under known conditions (e.g., Swart et al., 2002; Cohen et al., 2004; Rosenheim et al., 2004). The unexplained range of elemental ratio-temperature relationships derived for different aragonite-secreting organisms, from mollusks to fish to corals to sclerosponges, and the existence of high amplitude, high frequency variations in elemental ratios that cannot be explained by temperature (e.g., Cohen et al., 2001; Meibom et al., 2004; Sinclair, 2005) underscores the our lack of a detailed understanding of the mineralization process and adds considerable uncertainty to the interpretation of proxy records. Here, the compositions of our experimentally precipitated aragonite are used to constrain the biomineralization process in scleractinian corals and, thereby, provide insights into the mechanisms responsible for producing the compositional cycles used to derive proxy records of SST from coral skeleton.

A 12-month record of Mg/Ca, Sr/Ca, and Ba/Ca ratios in *D. labyrinthiformis* (brain coral) skeleton collected on Bermuda is shown in Fig. 12 (dotted curves). All of these

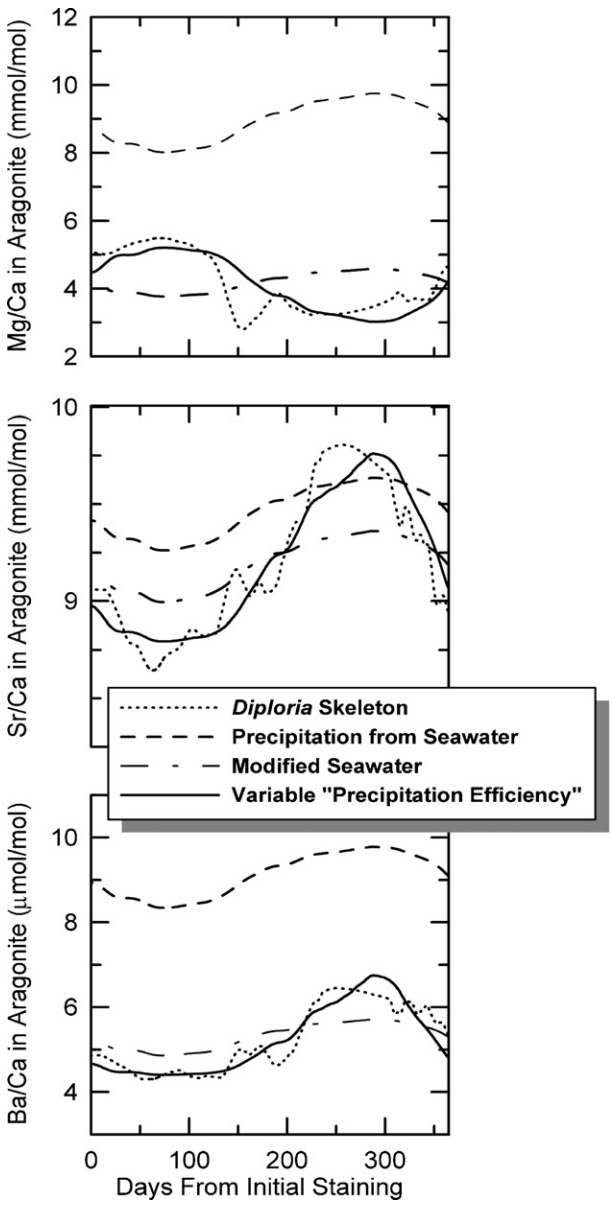

Fig. 12. Comparisons of 12-month records for Mg/Ca, Sr/Ca, and Ba/Ca ratios of *D. labyrinthiformis* skeleton from Bermuda (dotted curves) with results from precipitation calculations carried out using the experimentally determined partition coefficients from this study. Calculations were carried out assuming that (1) *Diploria* precipitates aragonite from seawater (dashed curves), and (2) from a calcifying fluid that is depleted in Mg, Sr, and Ba relative to seawater (dash-dot curves). A third set of calculations assumes that *Diploria* precipitates aragonite from a calcifying fluid that is compositionally distinct from seawater, and that the mass fraction of aragonite precipitated from the calcifying fluid varies systematically over the course of the year (solid curves).

elemental ratios exhibit annual cycles in the aragonite: the Mg/Ca ratio oscillates between ~3.2 and 5.5 mmol/mol, the Sr/Ca ratio between ~8.6 and 9.8 mmol/mol, and Ba/Ca ratios between ~4.3 and 6.4 μmol/mol. There is a positive correlation between sea surface temperature (SST) and the Mg/Ca variations in the coral skeleton, and negative correlations with both Sr/Ca and Ba/Ca ratios. To determine the extent to which these cycles could have been produced through precipitation of carbonate directly from seawater, without the influence of "vital effects," we used partition coefficients from our experiments (Table 5) and satellite-derived biweekly SSTs for a $1° \times 1°$ grid square centered on Bermuda (http://iridl.ldeo.columbia.edu/SOURCES/.IGOSS) for the time period represented by the coral data to model aragonite precipitation (dashed curves in Fig. 12). The annual cycle calculated for Mg/Ca is significantly offset from that found in the *Diploria* skeleton, with a mean ratio that is approximately twice that of the coral (9.0 versus 4.2 mmol/mol). The response of Mg/Ca to temperature predicted by the model is opposite to that in the coral (−0.193 versus 0.231 mmol/mol per °C). Results from the Sr/Ca calculations are more similar to the compositional variability in the *Diploria* aragonite, although the average Sr/Ca ratio for the model is slightly higher (9.5 versus 9.2 mmol/mol), and the temperature dependence is weaker (−0.042 versus −0.096 mmol/mol per °C). The mean Ba/Ca ratio predicted by the calculations is significantly higher than that of the *Diploria* skeleton (9.1 versus 5.3 μmol/mol), but the temperature dependencies are similar (−0.161 versus −0.213 μmol/mol per °C). This disagreement between the calculation results and annual cycles in the *Diploria* skeleton indicates the nature and magnitude of the "vital effect" on coral skeletal composition caused by modification of fluid composition during the biomineralization process.

To determine the extent to which *Diploria* modifies the composition of the calcifying fluid, we carried out calculations in which the concentrations of Mg, Sr, and Ba were decreased relative to Ca. Precipitation of aragonite from fluid with a Mg/Ca ratio of 2.5 mol/mol, a Sr/Ca ratio of 8.2 mmol/mol, and a Ba/Ca ratio of 3.0 μmol/mol produces annual cycles with mean ratios comparable to those of the coral skeleton. Although seawater is likely transported into the calcifying space at the start of the mineralization process (Cohen and McConnaughey, 2003; Braun and Erez, 2004), its composition is substantially modified prior to aragonite precipitation. This is a clear indication that physiology plays a prominent role in establishing the composition of biogenic aragonite. That the inferred decreases in the Mg/Ca, Sr/Ca, and Ba/Ca ratios of the putative calcifying fluid are different (Mg/Ca decreases by ~53%; Sr/Ca decreases by ~3%; Ba/Ca decreases by ~42% relative to seawater) indicates that they do not result simply from the selective addition of Ca^{2+} into the calcifying fluid. It is possible that lowered Mg/Ca, Sr/Ca, and Ba/Ca ratios in the calcifying fluid are a consequence of proton pumping which enhances aragonite precipitation rates by elevating local pH (Al-Horani et al., 2003). The Ca-ATPase enzyme pump is thought to transport one Ca^{2+} ion into the calcifying space for every two protons transported away (Cohen and McConnaughey, 2003). In addition, it is thought that Ca^{2+} may be transported via ion channels across the basal epithelium (Gattuso et al., 1999). The large discrepancy in the cationic radii of Mg^{2+} and Ba^{2+} relative to Ca^{2+} may mean that enzymes and ion channels can easily block or

select against them, preferentially transporting Ca^{2+} to the calcification site. Conversely, Sr^{2+} and Ca^{2+} are similar enough in size that there is little discrimination between the two during cross-membrane transport. As a result, the Sr/Ca ratio of the calcifying fluid remains comparable to that of seawater.

While the average composition of the *Diploria* skeleton can be explained by appealing to a calcifying fluid that is compositionally distinct from seawater, the amplitude of the Mg/Ca, Sr/Ca, and Ba/Ca annual cycles cannot. The most striking example of this is Mg/Ca, which responds to temperature in a manner opposite to that inferred from abiogenic aragonite. There are several potential explanations for these differences. First, it is possible that systematic variations in precipitation rate over the course of the year produce variable partition coefficients, amplifying the effects of temperature on the composition of the aragonite. However, this requires not only that the response of Mg^{2+} partitioning to precipitation rate is exceedingly strong, but also opposite to the response shown by Sr^{2+} and Ba^{2+} partitioning. Although both positive and negative precipitation rate dependencies have been identified experimentally for cation partitioning between calcite and aqueous fluid (Lorens, 1981; Tesoriero and Pankow, 1996), no systematic differences among the partitioning of Mg^{2+}, Sr^{2+}, and Ba^{2+} are apparent in our experimental results for aragonite. Although it cannot be ruled out at this point, a precipitation rate explanation seems unlikely.

A second potential mechanism for producing the compositional variations in the *Diploria* skeleton is a systematic variation in the composition of the calcifying fluid over the course of the year. This possibility was investigated by assuming that the concentrations of Mg, Sr, and Ba vary linearly, relative to Ca, in response to temperature. Results from these calculations demonstrate that such fluctuations, coupled with the inherent temperature dependence of the partition coefficients, are capable of explaining the *Diploria* data. This explanation requires that the Sr/Ca ratio of the calcifying fluid is nearly identical to that of seawater during the winter months, but that it decreases substantially in the summer. Likewise, the Ba/Ca ratio of the fluid is highest in the winter, and decreases significantly during the summer months. Conversely, this model calls for the Mg/Ca ratio of the calcifying fluid to behave antithetically to both Sr/Ca and Ba/Ca ratios: it is depressed in the summer and elevated during the winter months. It is not clear that this should be the case. Unlike calcite, aragonite precipitation is not inhibited by the high Mg/Ca ratio of seawater, making it unlikely that relatively small modulations in Mg would be necessary to enhance calcification (Morse et al., 1997; Davis et al., 2000). It is possible that algal symbiosis is somehow involved in increasing the Mg/Ca ratio of the calcifying fluid during the summer months, as Mg^{2+} is the centrally chelated ion in the chlorophyll molecule. However, SIMS analyses of Mg/Ca ratios in aragonite from asymbiotic corals exhibit both positive (Cohen et al., 2006) and negative temperature dependencies (A.L. Cohen, unpublished data). Therefore, while seasonal variations in the Mg/Ca, Sr/Ca, and Ba/Ca ratios of the calcifying fluid can explain the skeletal composition of *Diploria*, there is no obvious mechanism for driving these changes.

The mechanism that best explains the exaggerated compositional cycles in the *Diploria* skeleton involves seasonal variations in the mass fraction of aragonite precipitated from the calcifying fluid (“precipitation efficiency”), driven by changes in saturation state. This may result from variations in the efficiency of the Ca-ATPase enzyme pump or ion channel transport in response to changes in light and/or temperature over the course of the year. Elemental fractionations during precipitation are driven both by contrasts in partitioning and by variations in the mass fraction of solid that precipitates. For a specific mass fraction of aragonite precipitated from the calcifying fluid, the Mg/Ca, Sr/Ca, and Ba/Ca ratios in the solid all decrease with

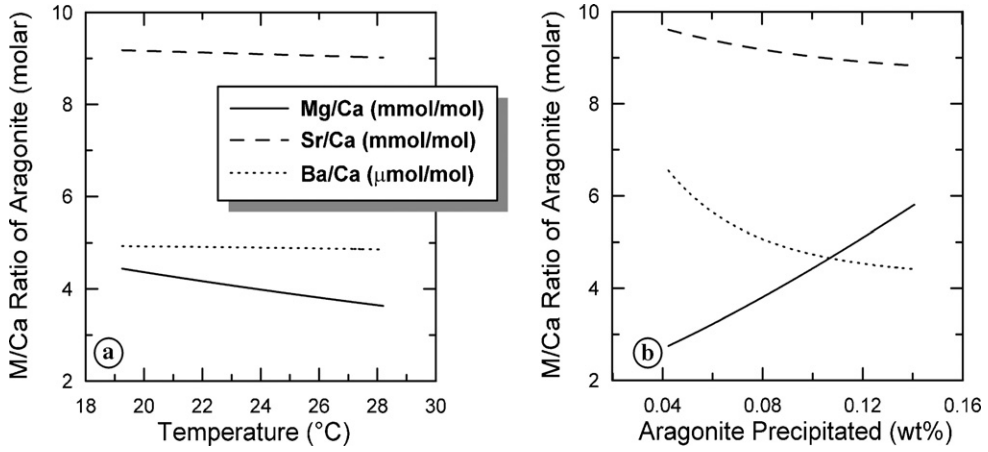

Fig. 13. Dependence of the composition of aragonite on (a) temperature and (b) weight percent of aragonite precipitated. Calculations were carried out for a putative*D. labyrinthiformis* calcifying fluid using the experimentally determined partition coefficients from this study. The weight percent of aragonite precipitated was assumed to be constant at 0.0883 in the temperature dependence calculations. The temperature was assumed to be constant at 23.16 °C for the mass precipitated calculations.

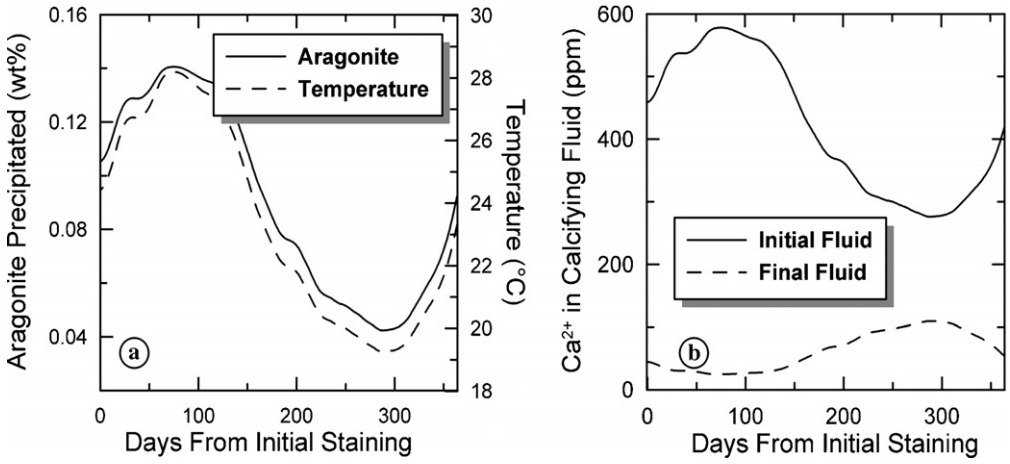

Fig. 14. (a) Seasonal variations in weight percent aragonite precipitated from putative *D. labyrinthiformis* calcifying fluid from variable "precipitation efficiency" calculations presented in Fig. 12. Also shown are the seasonal SST variations used to carry out the calculations. (b) Seasonal variations in concentration of Ca^{2+} in putative *D. labyrinthiformis* calcifying fluid before ("initial") and after ("final") aragonite precipitation from variable "precipitation efficiency" calculations presented in Fig. 12. Aragonite precipitation would be represented by vertical, downward-pointing vectors on this diagram. Replenishment of the calcifying fluid would be represented by upward-pointing vertical vectors.

increasing temperature due to changes in the aragonite-seawater partition coefficients (Fig. 13a). Conversely, at a given temperature (i.e. constant partition coefficients), the Sr/Ca and Ba/Ca ratios of the solid decrease while the Mg/Ca ratio increases as the "precipitation efficiency" increases, reflecting progressive changes in the composition of the residual calcifying fluid (Fig. 13b). Results from precipitation calculations demonstrate that the combined effects of temperature on element partitioning and an increase in "precipitation efficiency" during the summer months, relative to the winter, produces exaggerated decreases in the Sr/Ca and Ba/Ca ratios of the skeleton, combined with an *increase* in the Mg/Ca ratio (Fig. 12). Allowing the mass fraction of aragonite precipitated to increase from 0.00042 at 19 °C to 0.00141 at 28 °C reproduces the compositional trends observed in the *Diploria* skeleton for a calcifying fluid with a Mg/Ca ratio of 1.65 mol/mol, and Sr/Ca ratio of 8.64 mmol/mol, and a Ba/Ca ratio of 4.22 μmol/mol (Fig. 14a). This model implies that skeletal growth proceeds by aragonite precipitation from an isolated reservoir of calcifying fluid that is subsequently flushed and replenished. Cohen et al. (2006) reached a similar conclusion for the cold-water scleractinian *Lophelia pertusa* on the basis of modeling of the Sr/Ca annual cycles, supplemented by a limited amount of Mg/Ca ratio data.

The capacity for corals to preferentially exclude Ba^{2+} from the calcifying fluid and for variations in temperature and "precipitation efficiency" to produce seasonal cycles in Ba/Ca have important implications for the interpretation of proxy records. Lea et al. (1989) established the Ba/Ca ratio of coral skeleton as a proxy for oceanic upwelling based on the observation that cold, deep waters contain more Ba^{2+} than warm surface waters. As Lea et al. (1989) pointed out, however, this interpretation implicitly assumes that the amount of Ba^{2+} substituting for Ca^{2+} in the aragonite lattice reflects only the increased Ba^{2+} content of the upwelled seawater. They also noted that the possibility of a temperature effect could not be entirely ruled out. This possibility can now be tested by quantitatively determining whether seasonal Ba/Ca variability exceeds that which can be explained by calcifying fluid with a constant Ba/Ca ratio. If the annual ranges in temperature and "precipitation efficiency" indicated by amplitude of Mg/Ca and Sr/Ca cycles in the coral skeleton are insufficient to explain the amplitude of Ba/Ca, it would imply that the increased Ba/Ca ratio of the upwelled water is reflected in the composition of the calcifying fluid.

Our modeling results, combined with those of Cohen et al. (2006), indicate that the compositional cycles in the aragonite skeletons of tropical and deep-water scleractinians are produced by a process that is primarily physicochemical in nature. The composition of the calcifying fluid is actively controlled by the polyp: seawater brought into the calcifying space is modified by selective transport of ions across the basal epithelium. While the concentrations of Mg^{2+}, Sr^{2+}, Ca^{2+}, and Ba^{2+} all appear to vary over the seasonal cycle, elemental ratios remain constant. The concentration of Ca^{2+} in the calcifying fluid is enriched by ~50% relative to seawater during the summer months, but depleted by a similar amount during the winter (Fig. 14b). These variations alone are unlikely to provide the supersaturation levels required for aragonite precipitation, suggesting that elevated carbonate ion concentrations in the fluid are driving calcification. This is consistent with the "McConnaughey model" in which elevated saturation states are produced through proton pumping by the enzyme Ca^{2+}-ATPase (Cohen and McConnaughey, 2003). Once the necessary supersaturation levels have been achieved in the calcifying fluid, nucleation and growth of aragonite proceeds. Compositional variations in the aragonite can be expected to occur on timescales of minutes to

years, depending on the rate at which the mass fraction of aragonite precipitated changes, and the rate at which the calcifying fluid is replenished. Therefore, this Rayleigh fractionation process is capable is explaining high-frequency compositional variability without appealing to influence of an organic matrix.

5. Conclusions

The Mg/Ca, Sr/Ca, and Ba/Ca ratios of experimentally precipitated aragonite correlate inversely with temperature at 15–75 °C. The Ba/Ca ratio has the strongest response to temperature. The experimentally determined aragonite–seawater partition coefficients for Mg^{2+}, Ca^{2+}, Sr^{2+}, and Ba^{2+} are not consistent with equilibrium. Rather, the process of surface entrapment can explain the compatibilities of these elements, and the systematic change in partitioning with temperature, during growth of the aragonite crystals. A comparison of the skeletal composition of *Diploria* from Bermuda with our experimentally determined partition coefficients indicate that the fluid from which coral skeleton precipitates has a Sr/Ca ratio close to that of seawater, but is depleted in both Mg and Ba. Further, there appear to be seasonal fluctuations in the mass of aragonite precipitated from a given mass of calcifying fluid, most likely driven by variations in efficiency of the Ca-ATPase enzyme pump or ion channel transport in response to changes in light and/or temperature. The combined effects of surface entrapment during aragonite growth and seasonal fluctuations in "precipitation efficiency" likely forms the basis for the temperature information recorded in the aragonite skeletons of Scleractinian corals.

Acknowledgments

We are grateful to D.W. Lea and an anonymous referee for providing thoughtful reviews. Discussions with D. McCorkle were particularly helpful for enhancing our rudimentary understanding of the carbonate chemistry of seawater. The authors are grateful to E.B. Watson for providing the code used to model surface entrapment, J. Blusztajn and D. Schneider for help with the ICP-MS analyses, J. Goudreau and W. Martin for carrying out TA and TCO_2 analyses, D. Wellwood for performing the salinity determinations, and G. Layne for helping whenever the 3f was particularly cranky. This work was supported by NSF Grants OCE-0347328, OCE-0402728, and OCE-0527350.

Associate editor: David W. Lea

Appendix A. Estimating variables for surface entrapment model calculations

Following Watson (2004), the form of $C_i(x)$ curves was assumed to be

$$C_i(x) = C_{0i}F^{\exp(x/l)}, \tag{A1.1}$$

where $C(x)_i$ is the concentration of element i at some distance x from the surface, C_{0i} is the concentration assuming equilibrium partitioning between solid and fluid at infinite distance from the surface, F is the surface enrichment factor, and l is the half width of the near-surface region (assumed to be 0.5 nm). The dependence of aragonite precipitation rate on saturation state in our experiments was estimated using the empirical rate equation with coefficients derived from the data of Burton and Walter (1987):

$$R = (\exp(10.4 - 2038/T))(\Omega - 1)^{0.063T - 17.0}, \quad 15\ ^\circ\mathrm{C} \leqslant T \leqslant 38\ ^\circ\mathrm{C} \tag{A1.2}$$

$$R = (\exp(10.4 - 2038/T))(\Omega - 1)^{2.5}, \quad T \geqslant 38\ ^\circ\mathrm{C}, \tag{A1.3}$$

where T is temperature in Kelvin. Crystal growth rate (V) was derived from precipitation rate by approximating spherulites as hemispheres:

$$V = \frac{\mathrm{d}r}{\mathrm{d}t} = \frac{2}{9}\pi R\left(\frac{3}{2}\pi R t\right)^{-2/3}, \tag{A1.4}$$

where r is radius, t is time, and R is precipitation rate. Eq. (A1.4) was evaluated by assuming a constant precipitation rate and setting t equal to 79.5% of the duration of a given experiment to correspond to the point at which half the mass of a spherulite had been precipitated. Given the lack of experimental determinations of cation diffusion in aragonite, lattice diffusivity was set equal to a down-temperature extrapolation of Sr diffusivity on calcite determined by Cherniak (1997); given that lattice diffusion is extremely sluggish at the temperatures of our experiments, this rough approximation has little effect on the outcome of the calculations.

Appendix B. Aragonite precipitation model calculations

Aragonite precipitation calculations were carried out as follows. Partition coefficients were calculated according to the following empirical relationships derived from our experimental data:

$$D_{\mathrm{Mg}}^{\mathrm{Aragonite/Fluid}} = 3.81 \times 10^{-3} \exp\left(\frac{1909}{T + 273.15}\right), \tag{A2.1}$$

$$D_{\mathrm{Ca}}^{\mathrm{Aragonite/Fluid}} = 2074 + 5.79 \cdot T, \tag{A2.2}$$

$$D_{\mathrm{Sr}}^{\mathrm{Aragonite/Fluid}} = 2930 - 11.71 \cdot T, \tag{A2.3}$$

$$D_{\mathrm{Ba}}^{\mathrm{Aragonite/Fluid}} = 3.18 \times 10^{-2} \exp\left(\frac{3635}{T + 273.15}\right), \tag{A2.4}$$

where T is temperature in Celsius. These partition coefficients were used to calculate the composition of aragonite coexisting with calcifying fluid at the temperature of interest using the solution of the Rayleigh distillation equation for the composition of the mean solid:

$$\bar{C}_i^{\mathrm{Aragonite}} = C_i^0 \frac{1 - FL^D}{1 - FL}, \tag{A2.5}$$

where C_i^0 is the concentration of element i in the initial calcifying fluid and FL is the mass fraction of calcifying fluid remaining following aragonite precipitation. The mass fraction of carbonate precipitation that resulted in the condition where the sum of $MgCO_3$, $CaCO_3$, $SrCO_3$, and $BaCO_3$ in the solid summed to 100% was taken as the correct amount. This approach for determining the amount of aragonite precipitated at a given temperature provided a good match when tested against our experiments.

The fluid composition used in the "seawater" calculations is that of Vineyard Sound seawater reported in Table 2. The calcifying fluid used in the "modified seawater" calculations contains 431 ppm Mg, 392 ppm Ca, 7.3 ppm Sr, and 5.7 ppb Ba. The following expressions were used in the calculations in which the fluid composition was allowed to vary as a function of temperature:

$$\mathrm{Mg} = \frac{0.08883}{4.8217 - 0.1134 \cdot T}, \tag{A2.6}$$

$$\mathrm{Ca} = 0.02803, \tag{A2.7}$$

$$\mathrm{Sr} = \frac{0.0005178}{0.7784 + 0.0110 \cdot T}, \tag{A2.8}$$

$$\mathrm{Ba} = \frac{5.034 \times 10^{-7}}{-0.0001 + 0.0769 \cdot T}, \tag{A2.9}$$

where concentration is in weight percent and temperature is in Celsius.

Variable "precipitation efficiency" calculations were carried out using Eqs. A2.1–A2.5 through a global minimization in which the concentrations of Mg, Sr, and Ba in the calcifying fluid, and the mass fraction of calcifying fluid remaining following aragonite precipitation [FL from Eq. (A2.5)] were allowed to vary in order to derive the best match to the composition of the *Diploria* skeleton. The functional form for FL was assumed to be

$$FL = c_1 + c_2 T + c_3 T^{-1} + c_4 T^2, \tag{A2.10}$$

where T is temperature in Kelvin. The base calcifying fluid composition derived from these calculations contains 392 ppm Mg, 392 ppm Ca, 7.4 ppm Sr, and 5.7 ppb Ba. While these concentrations vary over the course of a year, the ratios remain constant. The coefficients derived for Eq. (A2.10) are as follows: $c_1 = 27.78$; $c_2 = -0.0911$; $c_3 = -2{,}622$; and $c_4 = 1.031 \times 10^{-4}$.

References

Al-Horani, F., Al-Moghrabi, S., de Beer, D., 2003. The mechanism of calcification and its relation to photosynthesis and respiration in the scleractinian coral *Galaxea fascicularis*. *Mar. Biol.* **142**, 419–426.

Albarede, F., Bottinga, Y., 1972. Kinetic disequilibrium in trace element partitioning between phenocrysts and host lava. *Geochim. Cosmochim. Acta* **36**, 141–156.

Alibert, C., Kinsley, L., Fallon, S.J., McCulloch, M.T., Berkelmans, R., McAllister, F., 2003. Source of trace element variability in Great Barrier Reef corals affected by the Burdekin flood plumes. *Geochim. Cosmochim. Acta* **67** (2), 231–246.

Bass, J.D., 1995. Elasticity of minerals, glasses and melts. In: Ahrens, T.J. (Ed.), *Mineral Physics and Crystallography: A Handbook of Physical Constants*. American Geophysical Union.

Beattie, P., 1994. Systematics and energetics of trace-element partitioning between olivine and silicate melts: implications for the nature of mineral/melt partitioning. *Chem. Geol.* **117**, 57–71.

Beck, J.W., Edwards, R.L., Ito, E., Taylor, F.W., Recy, J., Rougerie, F., Joannot, P., Henin, C., 1992. Sea-surface temperature from coral skeletal strontium/calcium ratios. *Science* **257** (5070), 644–647.

Beck, J.W., Recy, J., Taylor, F., Edwards, R.L., Cabioch, G., 1997. Abrupt changes in early Holocene tropical sea surface temperature derived from coral records. *Nature* **385** (6618), 705–707.

Blundy, J.D., Wood, B.J., 1994. Prediction of crystal-melt partition coefficients from elastic moduli. *Nature* **372**, 452–454.

Braun, A., Erez, J., 2004. Preliminary observations on sea water utilization during calcification in scleractinian corals. *Eos. Trans. AGU* **85** (47). Abstract B14B–04.

Brice, J.C., 1975. Some thermodynamic aspects of the growth of strained crystals. *J. Cryst. Growth* **28**, 249–253.

Burton, E.A., Walter, L.M., 1987. Relative precipitation rates of aragonite and Mg calcite from seawater: temperature or carbonate ion control? *Geology* **15**, 111–114.

Cherniak, D.J., 1997. An experimental study of strontium and lead diffusion in calcite, and implications for carbonate diagenesis and metamorphism. *Geochim. Cosmochim. Acta* **61** (19), 4173–4179.

Cohen, A.L., Gaetani, G.A., Lundälv, T., Corliss, B.H., George, R.Y., 2006. Compositional variability in the cold-water scleractinian, *Lophelia pertusa*: new insights into "vital" effects. *Geochem. Geophys. Geosys.* in press.

Cohen, A.L., Layne, G.D., Hart, S.R., Lobel, P.S., 2001. Kinetic control of skeletal Sr/Ca in a symbiotic coral: implications for the paleotemperature proxy. *Paleoceanography* **16** (1), 20–26.

Cohen, A.L., McConnaughey, T.A., 2003. Geochemical perspectives on coral mineralization. *Rev. Mineral Geochem.* **54**, 151–187.

Cohen, A.L., Owens, K.E., Layne, G.D., Shimizu, N., 2002. The effect of algal symbionts on the accuracy of Sr/Ca paleotemperatures from coral. *Science* **296** (5566), 331–333.

Cohen, A.L., Reves-Sohn, R.A., 2004. Tidal Modulation of Sr/Ca in a Pacific Reef Coral. *Geophys. Res. Lett.* **31**, L16310.

Cohen, A.L., Smith, S.R., McCartney, M.S., van Etten, J., 2004. How brain corals record climate: an integration of skeletal structure, growth and chemistry of *Diploria labyrinthiformis* from Bermuda. *Mar. Ecol. Prog. Ser.* **271**, 147–158.

Correge, T., Gagan, M., Beck, J., Burr, G., Cabioch, G., Le Cornec, F., 2004. Interdecadal variation in the extent of South Pacific tropical waters during the Younger Dryas event. *Nature* **428**, 927–929.

Davis, K.J., Dove, P.M., De Yoreo, J.J., 2000. The role of Mg^{2+} as an impurity in calcite growth. *Science* **290**, 1134–1137.

de Villiers, S., Shen, G.T., Nelson, B.K., 1994. The Sr/Ca-temperature relationship in coralline aragonite: influence of variability in $(Sr/Ca)_{seawater}$ and skeletal growth parameters. *Geochim. Cosmochim. Acta* **58** (1), 197–208.

Denbigh, K., 1981. *The Principles of Chemical Equilibrium*. Cambridge University Press, Cambridge.

Dietzel, M., Gussone, N., Eisenhauer, A., 2004. Co-precipitation of Sr^{2+} and Ba^{2+} with aragonite by membrane diffusion of CO_2 between 10 and 50 °C. *Chem. Geol.* **203**, 139–151.

Doerner, H.A., Hoskins, W.M., 1925. Co-precipitation of radium and barium sulfates. *J. Am. Chem. Soc.* **47**, 662–675.

Felis, T., Lohmann, G., Kuhnert, H., Lorenz, S.J., Scholz, D., Paetzold, J., Al-Rousan, S.A., Al-Moghrabi, S.M., 2004. Increased seasonality in Middle East temperatures during the last interglacial period. *Nature* **429** (6988), 164–168.

Gattuso, J.P., Allemand, D., Frankignoulle, M., 1999. Photosynthesis and calcification at cellular, organismal and community levels in coral reefs: A review on interactions and control by carbonate chemistry. *Am. Zoolog.* **39**, 160–183.

Gieskes, J.M., Rogers, W.C., 1973. Alkalinity determination in interstitial waters of marine sediments. *J. Sediment. Petrol.* **43**, 272–277.

Guilderson, T.P., Fairbanks, R.G., Rubenstone, J.L., 1994. Tropical temperature variations since 20,000 years ago: modulating interhemispheric climate change. *Science* **263** (5147), 663–665.

Hart, S.R., Cohen, A.L., 1996. An ion probe study of annual cycles of Sr/Ca and other trace elements in corals. *Geochim. Cosmochim. Acta* **60** (16), 3075–3084.

Hiraga, T., Anderson, I.M., Kohlstedt, D.L., 2004. Grain boundaries as reservoirs of incompatible elements in the Earth's mantle. *Nature* **427**, 699–703.

Holland, H.D., Borcsik, M., Munoz, J., Oxburgh, U.M., 1963. The coprecipitation of Sr^{2+} with aragonite and of Ca^{2+} with strontianite between 90 and 100 °C. *Geochim. Cosmochim. Acta* **27**, 957–977.

Joesten, R., 1991. Grain-boundary diffusion kinetics in silicate and oxide minerals. In: Ganguly, J. (Ed.), *Diffusion, atomic ordering, and mass transport: selected topics in geochemistry*. Springer-Verlag, pp. 345–395.

Kinsman, D.J.J., Holland, H.D., 1969. The coprecipitation of cations with $CaCO_3$: IV. The coprecipitation of Sr^{2+} with aragonite between 16 and 96 °C. *Geochim. Cosmochim. Acta* **33**, 1–17.

Kitano, Y., Kanamori, N., Oomori, T., 1971. Measurements of distribution coefficients of strontium and barium between carbonate precipitate and solution—abnormally high values of distribution coefficients measured at early stages of carbonate formation. *Geochem. J.* **4**, 183–206.

Lea, D.W., 2003. Elemental and isotopic proxies of marine temperature. In: Elderfield, H. (Ed.), *The Oceans and Marine Geochemistry*, vol. 6. Elsevier-Pergammon, pp. 365–390.

Lea, D.W., Shen, G.T., Boyle, E.A., 1989. Coralline barium records temporal variability in Equatorial Pacific upwelling. *Nature* **340**, 373–376.

Lorens, R.B., 1981. Sr, Cd, Mn and Co distribution coefficients in calcite as a function of calcite precipitation rate. *Geochim. Cosmochim. Acta* **45**, 553–561.

McCulloch, M., Fallon, S., Wyndham, T., Hendy, E., Lough, J., Barnes, D., 2003. Coral record of increased sediment flux to the inner Great Barrier Reef since European settlement. *Nature* **421** (6924), 727–730.

Meibom, A., Cuif, J.-P., Hillion, F., Constantz, B.R., Juillet-Leclerc, A., Dauphin, Y., Watanabe, T., Dunbar, R.B., 2004. Distribution of magnesium in coral skeleton. *Geophys. Res. Lett.* **31**, L23306.

Millero, F.J., Graham, T.B., Huang, F., Bustos-Serrano, H., Pierrot, D., 2006. Dissociation constants of carbonic acid in seawater as a function of salinity and temperature. *Mar. Chem.* **100** (1-2), 80–94.

Min, G.R., Edwards, R.L., Taylor, F.W., Recy, J., Gallup, C.D., Beck, J.W., 1995. Annual cycles of U/Ca in coral skeletons and U/Ca thermometry. *Geochim. Cosmochim. Acta* **59** (10), 2025–2042.

Mitsuguchi, T., Matsumoto, E., Abe, O., Uchida, T., Isdale, P.J., 1996. Mg/Ca thermometry in coral skeletons. *Science* **274** (5289), 961–963.

Morse, J.W., Wang, Q., Tsio, M.Y., 1997. Influences of temperature and Mg:Ca ratio on $CaCO_3$ precipitates from seawater. *Geology* **25** (1), 85–87.

Mucci, A., Canuel, R., Zhong, S., 1989. The solubility of calcite and aragonite in sulfate-free seawater and the seeded growth kinetics and composition of the precipitates at 25 °C. *Chem. Geol.* **74** (3–4), 309–320.

Nagasawa, H., 1966. Trace element partition coefficient in ionic crystals. *Science* **152**, 767–769.

Nordstrom, D.K., Plummer, L.N., Langmuir, D., Busenberg, E., May, H.M., Jones, B.F., Pankhurst, 1990. Revised chemical equilibrium data for major water–mineral reactions and their limitations. In: Melchior, D.C., Bassett, R.L. (Eds.), *Chemical Modeling of Aqueous Systems II*. American Chemical Society, Washington, DC.

O'Sullivan, D.W., Millero, F.J., 1998. Continual measurement of the total inorganic carbon in surface seawater. *Mar. Chem.* **60**, 75–83.

Onuma, N., Higuchi, H., Wakita, H., Nagasawa, H., 1968. Trace element partition between two pyroxenes and the host lava. *Earth Planet Sci. Lett.* **5**, 47–51.

Plummer, L.N., Busenberg, E., 1987. Thermodynamics of aragonite–strontianite solid solutions: results from stoichiometric solubility at 25 and 76 °C. *Geochim. Cosmochim. Acta* **51** (6), 1393–1411.

Reuer, M.K., Boyle, E.A., Cole, J.E., 2003. A mid-twentieth century reduction in tropical upwelling inferred from coralline trace element proxies. *Earth Planet Sci. Lett.* **210**, 437–452.

Rimstidt, J.D., Balog, A., Webb, J., 1998. Distribution of trace elements between carbonate minerals and aqueous solutions. *Geochim. Cosmochim. Acta* **62**, 1851–1863.

Rosenheim, B.E., Swart, P.K., Thorrold, S.R., Willenz, P., Berry, L., Latkoczy, C., 2004. High-resolution Sr/Ca records in sclerosponges calibrated to temperature in situ. *Geology* **32** (2), 145–148.

Schrag, D.P., 1999. Rapid analysis of high-precision Sr/Ca ratios in corals and other marine carbonates. *Paleoceanography* **14** (2), 97–102.

Shannon, R.D., 1976. Revised effective ionic radii and systematic studies of interatomic distances in halides and chalcogenides. *Acta Crystallogr.* **A32**, 751–767.

Shen, G.T., Dunbar, R.B., 1995. Environmental controls on uranium in reef corals. *Geochim. Cosmochim. Acta* **59** (10), 2009–2024.

Sinclair, D.J., 2005. Correlated trace element "vital effects" in tropical corals: a new geochemical tool for probing biomineralization. *Geochim. Cosmochim. Acta* **69**, 3265–3284.

Smith, S.V., Buddemeier, R.W., Redalje, R.C., Houck, J.E., 1979. Strontium-calcium thermometry in coral skeletons. *Science* **204** (4391), 404–407.

Smyth, J.R., Bish, D.L., 1988. *Crystal Structures and Cation Sites of Teh Rock-forming Minerals*. Allen and Unwin, London.

Stoll, H.M., Rosenthal, Y., Falkowski, P., 2002. Climate proxies from Sr/Ca of coccolith calcite: calibrations from continuous culture of *Emiliania huxleyi*. *Geochim. Cosmochim. Acta* **66** (6), 927–936.

Swart, P.K., Elderfield, H., Greaves, M.J., 2002. A High-resolution calibration of Sr/Ca thermometry using the Caribbean coral *Montastrea annularis*. *Geochem. Geophys. Geosys.* **3**, 8402, doi:10.1029/2002GC000306.

Tesoriero, A.J., Pankow, J.F., 1996. Solid solution partitioning of Sr^{2+}, Ba^{2+}, and Cd^{2+} to calcite. *Geochim. Cosmochim. Acta* **60**, 1053–1063.

Tiller, W.A., Jackson, K.A., Rutter, J.W., Chalmers, B., 1953. The redistribution of solute atoms during the solidification of metals. *Acta Metall.* **1**, 428–437.

Tudhope, A.W., Chilcott, C.P., McCulloch, M.T., Cook, E.R., Chappell, J., Ellam, R.M., Lea, D.W., Lough, J.M., Shimmield, G.B., 2001. Variability in the El Nino-Southern Oscillation through a glacial–interglacial cycle. *Science* **291** (5508), 1511–1517.

Wang, Y., Xu, H., 2001. Prediction of trace metal partitioning between minerals and aqueous solutions: a linear free energy correlation approach. *Geochim. Cosmochim. Acta* **65**, 1529–1543.

Watanabe, T., Winter, A., Oba, T., 2001. Seasonal changes in sea surface temperature and salinity during the Little Ice Age in the Caribbean Sea deduced from Mg/Ca and $^{18}O/^{16}O$ ratios in corals. *Mar. Geol.* **173** (1-4), 21–35.

Watson, E.B., 1996. Surface enrichment and trace-element uptake during crystal growth. *Geochim. Cosmochim. Acta* **60**, 5013–5020.

Watson, E.B., 2004. A conceptual model for near-surface kinetic controls on the trace-element and stable isotope composition of abiogenic calcite crystals. *Geochim. Cosmochim. Acta* **68**, 1473–1488.

Watson, E.B., Liang, Y., 1995. A simple model for sector zoning in slowly grown crystals: implications for growth rate and lattice diffusion, with emphasis on accessory minerals in crustal rocks. *Am. Mineral.* **80**, 1179–1187.

Winter, A., Ishioroshi, H., Watanabe, T., Oba, T., Christy, J., 2000. Caribbean Sea surface temperatures: two-to-three degrees cooler than present during the Little Ice Age. *Geophys. Res. Lett.* **27** (20), 3365–3368.

Wood, B.J., Blundy, J.D., 1997. A predictive model for rare earth element partitioning between clinopyroxene and anhydrous silicate melt. *Contrib. Mineral. Petrol.* **129**, 166–181.

Zhong, S., Mucci, A., 1989. Calcite and aragonite precipitation from seawater solutions of various salinities: precipitation rates and overgrowth compositions. *Chem. Geol.* **78**, 283–299.